J. Fluid Mech. (2024), *vol*. 1001, A55, doi:10.1017/jfm.2024.1148

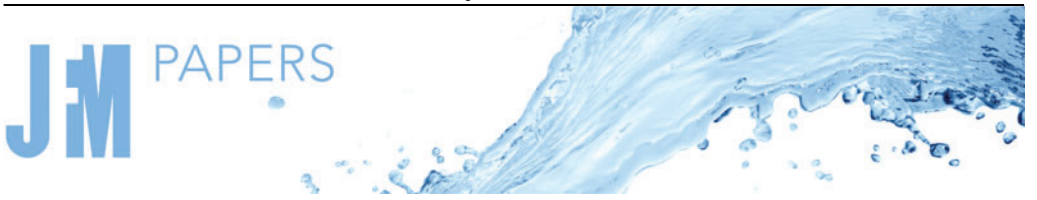

Internally heated convection with rotation: bounds on heat transport

Ali Arslan†

Institute of Geophysics, ETH Zürich, Zürich, CH-8092, Switzerland

(Received 17 June 2024; revised 14 October 2024; accepted 26 November 2024)

This work investigates heat transport in rotating internally heated convection, for a horizontally periodic fluid between parallel plates under no-slip and isothermal boundary conditions. The main results are the proof of lower bounds on the mean temperature, $\overline{\langle T \rangle}$, and the heat flux out of the bottom boundary, $\mathcal{F}_B$, at infinite Prandtl number, where the Prandtl number is the non-dimensional ratio of viscous to thermal diffusion. The lower bounds are functions of the Rayleigh number quantifying the ratio of internal heating to diffusion and the Ekman number, E, which quantifies the ratio of viscous diffusion to rotation. We utilise two different estimates on the vertical velocity, w, one pointwise in the domain (Yan, *J. Math. Phys.*, vol. 45(7), 2004, pp. 2718–2743) and the other an integral estimate over the domain (Constantin *et al.*, *Phys.* D*: Non. Phen.*, vol. 125, 1999, pp. 275–284), resulting in bounds valid for different regions of buoyancy-to-rotation dominated convection. Furthermore, we demonstrate that similar to rotating Rayleigh–Bénard convection, for small E, the critical Rayleigh number for the onset of convection asymptotically scales as $E^{-4/3}$.

Key words: Bénard convection, variational methods

1. Introduction

Heat transport by turbulent convection remains a pertinent area of research in both astrophysical and geophysical fluid dynamics. While boundary-forced thermal convection has been studied extensively, convection driven by internal heating has been relatively overlooked (Doering 2020). Nevertheless, internally heated convection (IHC) plays a significant role within planetary bodies, such as in the Earth's mantle and core, where the radioactive decay of isotopes and secular cooling drive fluid motion (Schubert, Turcotte & Olson 2001; Schubert 2015). Similarly, for stars, convective zones are driven by radiation

† Email address for correspondence: ali.arslan@erdw.ethz.ch

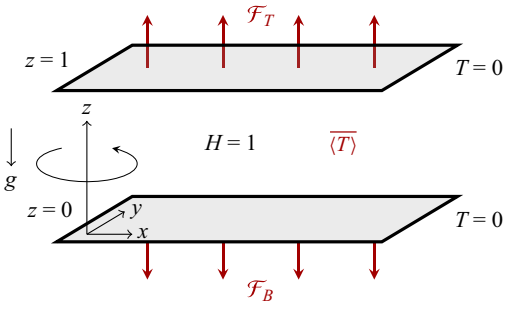

Figure 1. A non-dimensional schematic diagram for rotating uniform IHC. The upper and lower plates are at the same temperature, and the domain is periodic in the x and y directions and rotates about the z axis. Here $\mathcal{F}_B$ and $\mathcal{F}_T$ are the mean heat fluxes out the bottom and top plates, $\overline{\langle T \rangle}$ is the mean temperature and g is the acceleration due to gravity.

from nuclear fusion (Schumacher & Sreenivasan 2020) and supernovae are modelled as fluids heated internally by neutrinos (Herant *et al.* 1994; Radice *et al.* 2016). Moreover, stars and planets are rotating bodies where the Coriolis force affects the flow dynamics significantly (Greenspan 1968).

Studying rotating turbulent convection is challenging because experiments and numerical simulations cannot reach parameter values of interest (Glatzmaier 2013). For example, in planetary mantles, the Prandtl number, Pr, the non-dimensional number quantifying the ratio of the viscous and thermal diffusivity, reaches values of 10^{23}, while the Rayleigh number, R, quantifying the ratio of thermal forcing to diffusion is at least 10^6 (Mulyukova & Bercovici 2020). In planetary cores, the Rayleigh number could be as high as 10^{26} (Schubert 2015). Furthermore, the Ekman number, E, representing the viscous to rotational forces, is estimated to be 10^{-15} in the Earth's core (Jones & Schubert 2015).

An alternative route for inquiry is a mathematically rigorous study of the equations describing rotating convection. Of interest is the regime where the solutions of the governing equations are turbulent, and a key question is on the long-time behaviour of the mean quantities of the flow as a function of the control parameters (Pr, R, E). In this study, we employ the *background field method* (Doering & Constantin 1992, 1994; Constantin & Doering 1995; Doering & Constantin 1996) to study the mean heat transport in IHC subject to rotation between parallel plates with isothermal and no-slip boundary conditions (figure 1). Unlike turbulent convection driven by boundary heating, i.e. Rayleigh–Bénard convection (RBC), there are no known rigorous results for turbulent IHC subject to rotation.

The influence of rotation alters turbulent convection and introduces new flow regimes and physics (see Ecke & Shishkina 2023 for a recent review). The flow features of rotating convection in a plane layer driven by boundary heating are well documented (Veronis 1959; Chandrasekhar 1961; Rossby 1969; Julien *et al.* 1996; Knobloch 1998; Vorobieff & Ecke 2002; Boubnov & Golitsyn 2012; Stevens *et al.* 2013), and some insight exists for non-uniform IHC (Barker, Dempsey & Lithwick 2014; Currie *et al.* 2020; Hadjerci *et al.* 2024). However, no study has explored the flow in rotating uniform IHC. The preceding studies show that rotation inhibits the onset of convective motion and stabilises the fluid, creating a bias in motion parallel to the axis of rotation. Further, an Ekman boundary layer exists, enhancing the mean vertical heat transport by Ekman pumping (Greenspan 1968). With sufficient thermal forcing, the $E - R$ parameter space contains two extreme flow states: if R is sufficiently larger than E^{-1}, then buoyancy dominates and rotation

plays little effect on the dynamics, whereas if E^{-1} is large relative to R, and the vertical velocity is nonzero, geostrophic turbulence occurs (Julien *et al.* 1996; Sprague *et al.* 2006). A wide range of flow features occurs in rotating convection including, cellular flows, Taylor columns, large-scale vortices and plume-dominated convection (Grooms *et al.* 2010; Julien *et al.* 2012; Stellmach *et al.* 2014; Aurnou, Horn & Julien 2020; Guzmán *et al.* 2020; Kunnen 2021; Song, Shishkina & Zhu 2024).

In addition to experimental and numerical studies on rotating RBC, there exist proofs of bounds with the background field method, on the enhancement of heat transport due to convection, quantified with the Nusselt number, Nu (Constantin, Hallstrom & Putkaradze 1999; Constantin, Hallstrom & Poutkaradze 2001; Doering & Constantin 2001; Yan 2004; Grooms & Whitehead 2014; Pachev *et al.* 2020). First introduced in the 1990s, the background field method provides a tool for proving bounds on the long-time averages of turbulence (Fantuzzi, Arslan & Wynn 2022). In its original formulation, the idea involves decomposing the flow variables into a fluctuating and background component satisfying the boundary conditions to construct a variational problem for bounding the turbulent dissipation. A bound is proven by solving the variational problem by choosing an appropriate background field and using elementary integral estimates. The method has been used successfully for many fluid flows, none more so than turbulent convection (Nobili 2023). Recent insight has shown that the background field method fits within the framework of the *auxiliary functional method* (Chernyshenko *et al.* 2014; Chernyshenko 2022), which can yield sharp bounds for well-posed ordinary differential equations (ODEs) and partial differential equation (PDEs) under technical conditions (Tobasco, Goluskin & Doering 2018; Rosa & Temam 2022).

A fundamental feature of the background field method is to work with energy balances from the governing equations. However, energy identities fail to capture the effects of rotation, apart from in the case of a fluid driven by rotating boundaries, like in Taylor–Couette flow (Constantin 1994; Ding & Marensi 2019; Kumar 2022). For convection subject to the Coriolis force, standard applications of the background field method do not give a bound on Nu that depends on E. One path for progress is in the limit of infinite Pr, where the momentum equation simplifies to a forced Stokes flow, leading to a diagnostic equation between the velocity and temperature, facilitating better estimates. Notably, without rotation ($E = \infty$), using the background field method, it was proven, up to constants and logarithms, that $Nu \leq Ra^{1/3}$ (Doering, Otto & Reznikoff 2006), where Ra is the Rayleigh number based upon the temperature difference between the boundaries, improving on the bound of $Nu \leq Ra^{1/2}$ valid at arbitrary Pr (Doering & Constantin 1996). Under rotation ($E < \infty$) at $Pr = \infty$, established results for RBC are illustrated in figure 2.

High Pr restricts the parameter space when modelling fluid flows. However, proving bounds in the limit of $Pr = \infty$ can be viewed as a first step towards establishing bounds valid for all Pr. Recent studies suggest that for any bound proven at infinite Pr in rotating RBC, a semi-analytic bound for finite Pr can be obtained under specific conditions (Tilgner 2022). The results in Tilgner (2022) indicate that the bounds for finite Pr are, to highest order, equivalent to the infinite Pr results of figure 2, with Ra, Pr and E corrections. The result is unsurprising since bounds at infinite Pr generally improve those obtained for finite Pr. At the level of the dynamical system, this can be understood as a consequence of the relative ease with which information is extracted from the turbulent attractor of infinite Pr system by bounding methods (Wang 2007).

When rotation dominates over buoyancy, heuristic arguments for RBC suggest that $Nu \sim E^{3/2}Ra^2$, at arbitrary Pr (King, Stellmach & Buffett 2013; Plumley & Julien 2019; Aurnou *et al.* 2020). Bounds that scale similarly to the physical arguments in the rapidly rotating

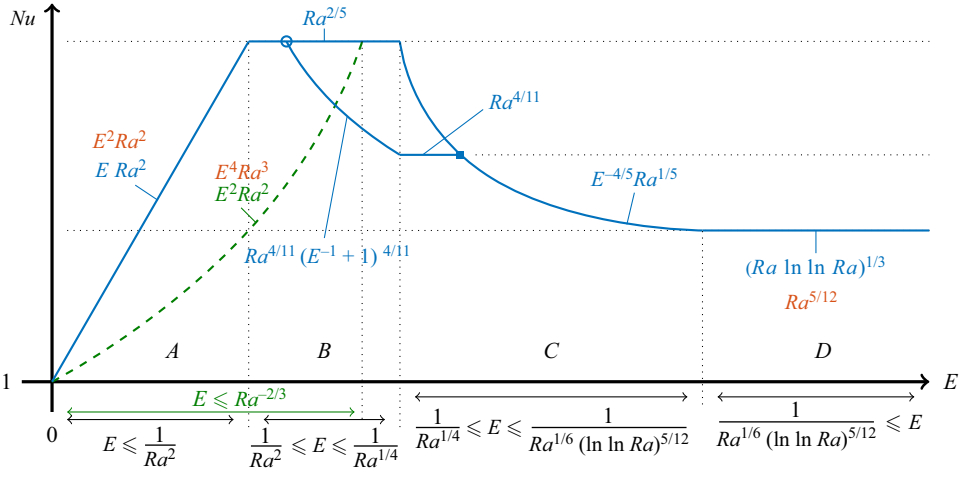

Figure 2. Illustration of the upper bounds with blue lines on the Nusselt number, Nu, in terms of the Rayleigh, Ra, and Ekman numbers, E, for infinite Prandtl number rotating RBC, between no-slip boundaries. All bounds hold up to constants that determine the exact sizes of the regions and where applicable red text shows the stress-free result in the same region. The bounds in A are due to Constantin *et al.* (1999). The green dashed line crossing A and B shows the upper bound obtained from the non-hydrostatic quasigeostrophic approximation (Grooms & Whitehead 2014; Pachev *et al.* 2020). In B, the crossover from the bound $Ra^{2/5}$ (Doering & Constantin 2001) to $Ra^{4/11}(E^{-1}+1)^{4/11}$ (Yan 2004) is shown by a blue circle. Similarly in region C the crossover from $Ra^{4/11}$ (Yan 2004) to $E^{-4/5}Ra^{1/5}$ (Constantin *et al.* 2001) is shown by a blue square. Region D shows the bounds for buoyancy-driven convection (Otto & Seis 2011; Whitehead & Doering 2011*b*). The transition from C to D is continuous up to logarithmic corrections (Constantin *et al.* 1999).

regime can be proven when working with an asymptotic approximation of the governing equations known as the non-hydrostatic quasigeostrophic (nhQG) equations (Julien *et al.* 1996, 2016). Scaling the horizontal length scales by $E^{1/3}$ and adjusting the time variable yields the nhQG equations that model the limit of rapidly rotating convection in a plane layer. Applying the background field method to the nhQG equations gives the green bounds in figure 2 of, up to constants, $Nu \leq E^2Ra^2$, for no-slip conditions (Pachev *et al.* 2020) and $Nu \leq E^4Ra^3$ for stress-free boundaries (Grooms & Whitehead 2014).

IHC remains less studied in part due to significant differences in the physics between RBC. Notably, in uniform IHC between isothermal boundaries, the mean conductive heat flux is zero, rendering the standard definition of the Nusselt number inapplicable (Goluskin 2015). In previous works with zero rotation (Goluskin 2015), an alternative measure of the turbulent convection is the non-dimensionalised mean temperature, $\overline{\langle T\rangle}$, where angled brackets $\langle\cdot\rangle$ denote a volume and overbars denote a long-time average. As the flow becomes increasingly turbulent, the temperature within the domain becomes homogenised, quantified in a lower value of $\overline{\langle T\rangle}$ and a higher proxy Nusselt number defined as $Nu_p = 1/\overline{\langle T\rangle}$. An additional measure of turbulence is $\overline{\langle wT\rangle}$, quantifying the portion of heat leaving through each boundary, $\mathcal{F}_T$ and $\mathcal{F}_B$, due to convection (Goluskin & Spiegel 2012). For a stationary fluid, the heat supplied leaves the domain symmetrically out of both boundaries to ensure the statistical stationarity of the solutions. As the thermal forcing increases, convection carries heat upwards, causing a higher portion of the heat to leave through the top relative to the bottom boundary (Goluskin & van der Poel 2016).

In line with previous works on uniform IHC (Goluskin 2015; Arslan *et al.* 2021*a*,*b*; Kumar *et al.* 2022; Arslan *et al.* 2023; Arslan & Rojas 2024), the non-dimensional heat

Region	Condition	Bound on $\mathcal{F}_B$	Condition	Bound on $\overline{\langle T\rangle}$
I	$E \gtrsim R^{-2}$ $E \in [E_m, E_0]$	$d_4R^{-2/3} + d_5R^{-1/2}\lvert\ln(1 - d_6R^{-1/3})\rvert$	$E \gtrsim R^{-2/3}$ $E \in [E_m, E_1]$	$d_{11}R^{-2/7}$
Ia			$E \gtrsim R^{-2/3}$ $E \geq E_m$	$d_{13}R^{-1}E^{-1}$
II	$E \lesssim R^{-2}$ $E \in [E_m, E_0]$	$\frac{1}{2}$	$E \lesssim R^{-2/3}$ $E \in [E_m, E_1]$	$\frac{1}{12}$
III	$E \gtrsim R^{-2}$ $E \leq E_0$	$d_1R^{-2/3}E^{2/3} + d_2R^{-1/2}E^{1/2}\lvert\ln(1 - d_3R^{-1/3}E^{1/3})\rvert$	$E \gtrsim R^{-5/9}$ $E \leq E_1$	$d_{10}R^{-2/7}E^{2/7}$
IIIa			$R^{-5/9} \gtrsim E \gtrsim R^{-2/3}$ $E \leq E_1$	$d_{13}R^{-1}E^{-1}$
IV	$E \lesssim R^{-2}$ $E \leq E_0$	$d_7R^{-1} + d_8R^{-4/5}\lvert\ln(1 - d_9R^{-2/5})\rvert$	$E \lesssim R^{-2/3}$ $E \leq E_1$	$d_{12}R^{-1/3}$

Table 1. Summary of the lower bounds on $\mathcal{F}_B$ and $\overline{\langle T\rangle}$ proven in this work. The constants in the bounds are collated in Appendix A for brevity, while $E_0 = 5.4927$, $E_1 = 8$ and $E_m = 41.4487$. Region I corresponds to buoyancy-dominated convection, region II corresponds to solid body rotation, region III corresponds to buoyancy or rotation-dominated convection and region IV corresponds to rotation-dominated convection provided $R > R_L(E)$ where R_L is the value of R above which the system is linearly unstable.

flux out of the top and bottom boundaries is given by

$$\mathcal{F}_T := -\overline{\langle \partial_z T\rangle_h}|_{z=1} = \tfrac{1}{2} + \overline{\langle wT\rangle}, \tag{1.1a}$$

and

$$\mathcal{F}_B := \overline{\langle \partial_z T\rangle_h}|_{z=0} = \tfrac{1}{2} - \overline{\langle wT\rangle}. \tag{1.1b}$$

The non-dimensionalisation sets the limits of $\overline{\langle wT\rangle}$ as 0 and $\frac{1}{2}$, with each limit corresponding to no convection and infinitely effective convection, respectively. We seek bounds of the form $\mathcal{F}_B \geq f_1(R, E)$ and $\overline{\langle T\rangle} \geq f_2(R, E)$ in different regions of E–R space, where f_1 and f_2 are functions of only R and E. In previous applications of the background field method to IHC, bounds for $\overline{\langle T\rangle}$ are proven with minor adaptation from the background field method as applied to RBC (Lu, Doering & Busse 2004; Whitehead & Doering 2011*a*, 2012). However, in the case of obtaining bounds on $\overline{\langle wT\rangle}$ and consequently $\mathcal{F}_B$, it has been established that the variational problem requires a minimum principle on T, which states that temperature in the domain is greater than or equal to zero (Arslan *et al.* 2021*b*). The minimum principle is necessary to obtain lower bounds on $\mathcal{F}_B$ that remain positive as R increases. In the case of no rotation at $Pr = \infty$, the best-known lower bound on the mean temperature, up to constants, are $\overline{\langle T\rangle} \geq (R \ln R)^{-1/4}$ (Whitehead & Doering 2011*a*) and $\overline{\langle T\rangle} \geq R^{-5/17}$ (Whitehead & Doering 2012) for no-slip and stress-free boundaries. Conversely, the best-known lower bounds on the heat flux out of the domain are $\mathcal{F}_B \geq R^{-2/3} + R^{-1/2}\lvert\ln(1 - R^{-1/3})\rvert$ and $\mathcal{F}_B \geq R^{-40/29} + R^{-35/29}\lvert\ln(1 - R^{-10/29})\rvert$ (Arslan & Rojas 2024) for the two different kinematic boundary conditions.

In this paper, the bounds we prove for uniform IHC subject to rotation at an infinite Prandtl number are summarised in table 1.

For notation, $\|f\|_p^p = \int_0^1 f^p \,\mathrm{d}z$, for $p < \infty$ and $\|f\|_\infty = \operatorname{ess\,sup}_{z\in[0,1]} f$ for $p = \infty$, represents the standard L^p norms of $f : [0, 1] \to \mathbb{R}$. The use of $\lesssim$ or $\gtrsim$ indicates equality up to an independent constant. This paper is structured as follows. In § 2, we describe the problem set-up before discussing the onset of convection in § 3. Then Appendix B

proposes heuristic scaling arguments for rotating IHC before we prove bounds on $\mathcal{F}_B$ in § 4 and on $\langle\overline{T}\rangle$ in § 5. Finally, § 6 offers a brief discussion and concluding remarks.

2. Set-up

We consider a layer of fluid in a rotating frame of reference between two horizontal plates separated by a distance d and periodic in the horizontal (x and y) directions with periods $L_x d$ and $L_y d$. The fluid has kinematic viscosity ν, thermal diffusivity κ, density ρ, specific heat capacity c_p and thermal expansion coefficient α. Gravity acts in the negative vertical direction with strength g, the fluid rotates at rate Ω and is uniformly heated internally at a volumetric rate H.

To non-dimensionalise the problem, we use d as the characteristic length scale, d^2/κ as the time scale and $d^2H/\kappa\rho c_p$ as the temperature scale (Roberts 1967). The velocity of the fluid $\boldsymbol{u}(\boldsymbol{x}, t) = u(\boldsymbol{x}, t)\boldsymbol{e}_1 + v(\boldsymbol{x}, t)\boldsymbol{e}_2 + w(\boldsymbol{x}, t)\boldsymbol{e}_3$ and temperature $T(\boldsymbol{x}, t)$ in the non-dimensional domain $V = [0, L_x] \times [0, L_y] \times [0, 1]$ are governed by the infinite Prandtl number Boussinesq equations,

$$\boldsymbol{\nabla} \cdot \boldsymbol{u} = 0, \tag{2.1a}$$

$$\boldsymbol{\nabla} p + E^{-1}\boldsymbol{e}_3 \times \boldsymbol{u} = \nabla^2 \boldsymbol{u} + RT\boldsymbol{e}_3, \tag{2.1b}$$

$$\partial_t T + \boldsymbol{u} \cdot \boldsymbol{\nabla} T = \nabla^2 T + 1. \tag{2.1c}$$

The non-dimensional numbers are the Ekman and Rayleigh numbers, defined as

$$E = \frac{\nu}{2\Omega d^2} \quad \text{and} \quad R = \frac{g\alpha H d^5}{\rho c_p \nu \kappa^2}. \tag{2.2a,b}$$

The boundary conditions are of no-slip and isothermal temperature, respectively:

$$\boldsymbol{u}|_{z=\{0,1\}} = 0, \tag{2.3a}$$

$$T|_{z=\{0,1\}} = 0. \tag{2.3b}$$

Figure 1 provides a schematic for the system under consideration. The vertical component of the curl and double curl of (2.1*b*) gives a diagnostic equation involving the vertical velocity w, the vertical vorticity ζ and temperature T:

$$\nabla^4 w = E^{-1}\partial_z \zeta - R\Delta_h T, \tag{2.4a}$$

$$\nabla^2 \zeta = -E^{-1}\partial_z w, \tag{2.4b}$$

where $\Delta_h = \partial_x^2 + \partial_y^2$ is the horizontal Laplacian.

The final ingredients are results from Yan (2004) and Constantin *et al.* (1999) and a minimum principle on T. We state the results as separate lemmas.

LEMMA 2.1 (Minimum principle). *Suppose $T(\boldsymbol{x}, t)$ solves (2.1c) subject to (2.3b) where $\boldsymbol{u}$ satisfies $\boldsymbol{\nabla} \cdot \boldsymbol{u} = 0$ and (2.3a). Let the negative parts of $T(\boldsymbol{x}, t)$ be*

$$T_-(\boldsymbol{x}, t) := \max\{-T(\boldsymbol{x}, t), 0\}. \tag{2.5}$$

Then

$$\langle |T_-(\boldsymbol{x}, t)|^2 \rangle \leq \langle |T_-(\boldsymbol{x}, 0)|^2 \rangle \exp(-\mu t), \tag{2.6}$$

for some $\mu > 0$. In particular, if $T(\boldsymbol{x}, 0) > 0$, then $T_-(\boldsymbol{x}, 0) = 0$ and $T(\boldsymbol{x}, t) \geq 0 \ \forall t$.

See Appendix A of Arslan *et al.* (2021*b*) for a proof.

LEMMA 2.2 (Yan (2004)). *Let $w_{\boldsymbol{k}}, T_{\boldsymbol{k}} : (0, 1) \to \mathbb{R}$, be the Fourier transforms of the vertical velocity w and temperature T with wavenumber $\boldsymbol{k} = (k_x, k_y)$ satisfying (2.4) and $\boldsymbol{\nabla} \cdot \boldsymbol{u} = 0$, subject to the velocity boundary conditions (2.3a). Then we have the following.*

- *For $|\boldsymbol{k}| \leq 1$*
$$\|w''_{\boldsymbol{k}}\|_\infty \leq c_1 R(1 + \tfrac{1}{4}E^{-2})^{1/4}\|T_{\boldsymbol{k}}\|_2, \tag{2.7}$$
where $c_1 = 6^{1/4}$.
- *For $|\boldsymbol{k}| \geq 1$*
$$\|w''_{\boldsymbol{k}}\|_\infty \leq c_2 R\sqrt{\boldsymbol{k}}\|T_{\boldsymbol{k}}\|_2 + c_2 RE^{-1}\|T_{\boldsymbol{k}}\|_2, \tag{2.8}$$
where $c_2 = 1 + ((e^2 + 1)/(e^2 - 1))((4\cosh 1 + 2\sinh 1)/(-1 + \sinh 1)) \sim 64.8734$.

LEMMA 2.3 (Constantin *et al.* (1999)). *Let $w, T : V \to \mathbb{R}$ be horizontally periodic functions such that they solve (2.4) subject to $\boldsymbol{\nabla} \cdot \boldsymbol{u} = 0$ and the boundary conditions (2.3a), then*
$$\langle|\nabla^2 w|^2\rangle + 2\langle|\boldsymbol{\nabla}\zeta|^2\rangle \leq R^2\langle|T|^2\rangle. \tag{2.9}$$

3. Onset of convection

Before proving bounds on the emergent properties of the turbulence ($\mathcal{F}_B$ and $\overline{\langle T\rangle}$), we briefly discuss the onset of convection for (2.1). The trivial solution of (2.1) is found by taking $\boldsymbol{u} = 0$ and considering a steady state where the temperature is independent of time. The conductive temperature profile,
$$T_c = \tfrac{1}{2}z(1 - z), \tag{3.1}$$
represents the transport of heat by conduction alone. In the case where there is no rotation ($E = \infty$) for the boundary conditions in (2.3), the system becomes linearly unstable for all $R > 37\,325.2$ (Goluskin 2015). However, unlike RBC when considering (2.1) in the form
$$\frac{\mathrm{d}\boldsymbol{s}}{\mathrm{d}t} + \mathcal{L}\boldsymbol{s} + \mathcal{N}(\boldsymbol{s}, \boldsymbol{s}) + \mathcal{P}p = 0, \tag{3.2}$$
where $\mathcal{L}$ and $\mathcal{P}$ are linear operators, $\mathcal{N}$ is a bilinear operator and $\boldsymbol{s} = (\boldsymbol{u}, T)$ is the state vector, the linear operator $\mathcal{L}$ of (2.1) has a non-zero skew-symmetric component and nonlinear instability can occur at $R = 26\,926.6$, implying that subcritical convection can occur for IHC (Straughan 2013; Goluskin 2015). For $E < \infty$, rotation stabilises the system to vertical motion and inhibits the onset of convection. For the case of RBC, the effect of rotation on the onset of convection is well quantified (Chandrasekhar 1961). In this section, we demonstrate a result for the effect of rotation on the Rayleigh number for linear instability, R_L, in IHC.

3.1. *Linear stability*

The Rayleigh number up to which the flow is linearly stable is identified by analysing the evolution of perturbations from the linearised system of (2.1). In the non-rotating case, for selected thermal boundary conditions, the marginally stable states are stationary

(Davis 1969; Herron 2003). When the flow is subject to rotation, the condition for steady rolls, as opposed to oscillatory-in-time rolls, at the onset of convection is unknown. For comparison, in the case of RBC, the onset modes are steady provided $Pr \geq 0.68$, such that assuming a sufficiently large Pr fluid removes the question of oscillatory motion in the analysis we carry out here. The precise structure of the motion at the onset should not affect the asymptotic behaviour of R_L for a small Ekman number. It is noteworthy that in the case of the rotating internally heated fluid sphere, the first convective modes are always unsteady (Roberts 1968; Busse 1970; Jones, Soward & Mussa 2000) and recent evidence from numerical simulations confirms the existence subcritical convection (Guervilly & Cardin 2016; Kaplan *et al.* 2017).

Taking the set-up as described in § 2, we start by decomposing the temperature field into perturbations from the conductive profile $T_c(z)$,

$$T(\boldsymbol{x}, t) = \vartheta(\boldsymbol{x}, t) + T_c(z), \tag{3.3}$$

to obtain the temperature perturbation, ϑ equation from (2.1*c*) and boundary conditions of

$$\partial_t \vartheta + \boldsymbol{u} \cdot \boldsymbol{\nabla} \vartheta = \nabla^2 \vartheta + T_c' w, \tag{3.4a}$$

$$\vartheta|_{z=\{0,1\}} = 0, \tag{3.4b}$$

where primes denote derivative with respect to z. Then, we look at the marginally stable stationary states of the linearised system of (2.1) by considering the z component of the double curl of the momentum equation and the vertical component of the vorticity equation; we thus have

$$\nabla^4 w = E^{-1} \partial_z \zeta - R \nabla_H^2 \vartheta, \tag{3.5a}$$

$$\nabla^2 \zeta = -E^{-1} \partial_z w, \tag{3.5b}$$

$$\nabla^2 \vartheta = T_c' w. \tag{3.5c}$$

Given horizontal periodicity, we take a Fourier series expansion in the horizontal (x and y) directions of the form,

$$\begin{bmatrix} \vartheta(x, y, z) \\ \boldsymbol{u}(x, y, z) \\ \zeta(x, y, z) \end{bmatrix} = \sum_{\boldsymbol{k}} \begin{bmatrix} \vartheta_{\boldsymbol{k}}(z) \\ \boldsymbol{u}_{\boldsymbol{k}}(z) \\ \zeta_{\boldsymbol{k}}(z) \end{bmatrix} \mathrm{e}^{\mathrm{i}(k_x x + k_y y)}, \tag{3.6}$$

where the sum is over wavevectors $\boldsymbol{k} = (k_x, k_y)$ with magnitude $k = \sqrt{k_x^2 + k_y^2}$ and variables with subscripts $\boldsymbol{k}$ are functions of z only. Then, substituting (3.6) into (3.5) gives

$$(D^2 - k^2)^2 w_{\boldsymbol{k}} = E^{-1} \zeta_{\boldsymbol{k}}' + R k^2 \vartheta_{\boldsymbol{k}}, \tag{3.7a}$$

$$(D^2 - k^2) \zeta_{\boldsymbol{k}} = -E^{-1} w_{\boldsymbol{k}}', \tag{3.7b}$$

$$(D^2 - k^2) \vartheta_{\boldsymbol{k}} = T_c' w_{\boldsymbol{k}}, \tag{3.7c}$$

where $D^2 = \mathrm{d}^2/\mathrm{d}z^2$. For no-slip or stress-free boundary conditions, $\zeta_{\boldsymbol{k}}$ and $\vartheta_{\boldsymbol{k}}$ can be eliminated from (3.7) to give

$$(D^2 - k^2)^3 w_{\boldsymbol{k}} + E^{-2} w_{\boldsymbol{k}}'' = R k^2 T_c' w_{\boldsymbol{k}}. \tag{3.8}$$

Here, (3.8) is an eigenvalue problem and can be solved numerically by fixing E and finding the R at which the first eigenvalue changes sign. The equivalent problem for

RBC is well documented (Chandrasekhar 1961), however unlike RBC, the ODE in (3.8) admits solutions which are hypergeometric functions because T_c in (3.1) is a non-constant function. As such, even in the case of stress-free boundary conditions where $w_k = w_k'' = w_k'''' = 0$ at both boundaries, (3.8) becomes complicated to solve. Instead, we consider the asymptotic regime of small E where a simplified form of (3.8) gives the desired asymptotic relation between R_L and E. Following the argument first presented in Chandrasekhar (1961), we posit that for R close to R_L, the wavenumber k tends to infinity so that we retain only terms in E, R and the highest power in k and (3.8) becomes

$$E^{-2}w_k'' = k^2(R(\tfrac{1}{2} - z) + k^4)w_k. \tag{3.9}$$

Since (3.9) is of second order, we require only two boundary conditions. However, in the simplest set of boundary conditions of stress-free boundaries where w_k and w_k'' are zero, the problem is over-determined with four boundary conditions. It suffices to take $w_k(0) = w_k''(0) = 0$, such that we can make the ansätz that

$$w_k = Ai(n - mz) - \frac{Ai(n)}{Bi(n)}Bi(n - mz), \tag{3.10}$$

where $Ai(z)$ and $Bi(z)$ are the Airy functions of the first and second kind. Substituting (3.10) back into (3.9) gives

$$E^{-2}m^2(n - mz) = \tfrac{1}{2}k^2R + k^6 - k^2Rz, \tag{3.11}$$

from which we require the choice that $m = (k^2RE^2)^{1/3}$. Substituting for m and rearranging, we obtain

$$-\tfrac{1}{2}E^{2/3}k^{2/3}R + nR^{2/3} - E^{2/3}k^{14/3} = 0. \tag{3.12}$$

Given that (3.12) is a cubic equation in $R^{1/3}$, by application of the cubic formula, we find the real root to be

$$R_L^{1/3} = \frac{2n}{3E^{2/3}k^{2/3}} + \frac{1}{3E^{2/3}k^{2/3}}\left(-8n^3 + 27E^2k^6 + 27E^2k^3\sqrt{k^6 - \frac{16n^3}{27E^2}}\right)^{1/3}$$
$$+ \frac{4n^2}{3E^{2/3}k^{2/3}}\left(-8n^3 + 27E^2k^6 + 27E^2k^3\sqrt{k^6 - \frac{16n^3}{27E^2}}\right)^{-1/3}. \tag{3.13}$$

Then, we want to find the smallest possible R_L in (3.13) by finding the minimising k by solving $\partial_k R_L^{1/3} = 0$ and substituting back into (3.13) to obtain R_L as a function of only E. In figure 3 we plot R_L from (3.13) against k for a wide range of E (10^{-37} to 10^{-13}), highlighting the minimum in k found. The inset in figure 3 demonstrates that the k_m varies as $E^{-1/3}$. Given figure 3, and noting that in the asymptotic limit of small E we assume large wavenumbers k, it is natural in (3.13) to take the minimising wavenumber to be

$$k_m^6 = \frac{16n^3}{27E^2}, \tag{3.14}$$

such that the terms in the cube roots are real and positive. Then, substituting k_m back into (3.13) and the minimal $R_L(n, E)$ is achieved with $n = 1$, such that (3.13) simplifies to

$$R_L = \frac{(1 + 2^{2/3} + 2^{4/3})^3}{9 \cdot 2^{1/3}}E^{-4/3} \sim E^{-4/3}. \tag{3.15}$$

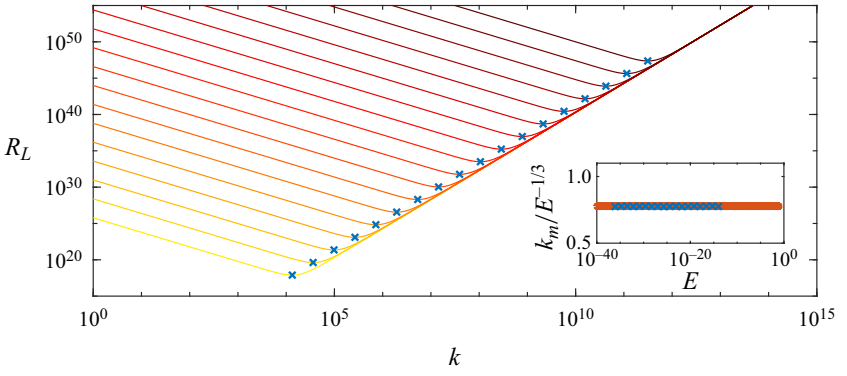

Figure 3. Plot of R_L against k as given by (3.13) for Ekman numbers ranging from 10^{-37} (red) to 10^{-13} (yellow). The blue dots represent the minimum R_L in k, and the inset demonstrates that the minimum wavenumber k_m varies as $E^{-1/3}$ with a compensated plot.

The asymptotic scaling is equivalent to rotating RBC, unsurprising given the equivalence of the momentum equations, albeit with different prefactors, and highlights the inhibiting effect of rotation on the Rayleigh number for the system to become linearly unstable. In the rest of the paper, we use (3.15) to arrive at heuristic scaling arguments and later contextualise the bounds proven.

4. Bounds on the heat flux out of the domain

In this section, we present proofs of the bounds in (1) on $\mathcal{F}_B$ as defined by (1.1). To obtain a lower bound on $\mathcal{F}_B$, we prove upper bounds on $\overline{\langle wT\rangle}$ by the background field method in the framework of auxiliary functionals (Arslan *et al.* 2023). First, in § 4.1, we derive the variational problem for finding U where $\overline{\langle wT\rangle} \leq U$. In § 4.2, we outline the preliminary choices that are made for the proofs and in § 4.3, estimate the upper bound on $\overline{\langle wT\rangle}$. Then, we first prove a bound on $\overline{\langle wT\rangle}$ valid for large Ekman numbers E in § 4.4 by the use of Lemma 2.2, followed by a proof valid for small E in § 4.5 by using Lemma 2.3. To provide an overview, figure 4 illustrates the lower bounds on $\mathcal{F}_B$, omitting the logarithmic corrections for brevity.

4.1. *The auxiliary functional method*

Here, we outline the main steps in constructing the variational problem to obtain an upper bound on $\overline{\langle wT\rangle}$. See previous works for a detailed derivation (Arslan *et al.* 2021*b*, 2023). To prove an upper bound on $\overline{\langle wT\rangle}$, we employ the auxiliary function method (Chernyshenko *et al.* 2014; Fantuzzi *et al.* 2022). The method relies on the observation that the time derivative of any bounded and differentiable functional $\mathcal{V}\{T(t)\}$ along solutions of the Boussinesq equations (2.1) averages to zero over infinite time, so that

$$\overline{\langle wT\rangle} = \overline{\langle wT\rangle + \frac{\mathrm{d}}{\mathrm{d}t}\mathcal{V}\{T(t)\}}. \tag{4.1}$$

Two key simplifications follow. The first is that we can estimate (4.1) by the pointwise-in-time maximum along the solutions of the governing equations, and this value is estimated by the maximum it can take over *all* velocity and temperature fields that are periodic in x and y, satisfying incompressibility (2.1*a*), the boundary conditions (2.3) and the maximum principle Lemma 2.1.

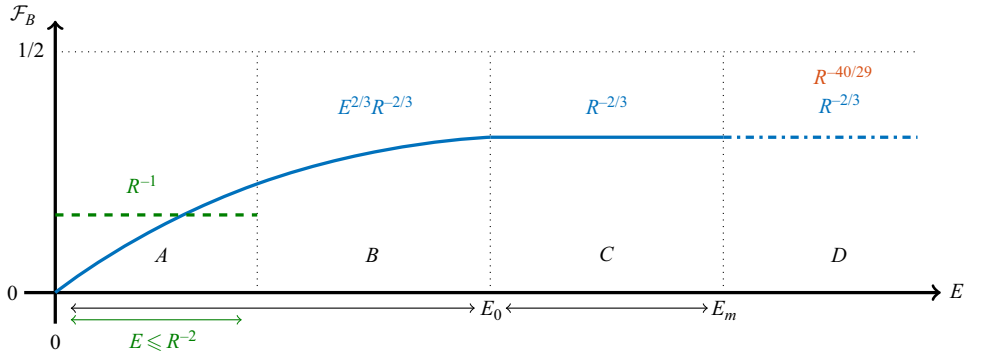

Figure 4. Illustrations of the lower bounds on the flux out of the bottom boundary, $\mathcal{F}_B$, between no-slip and isothermal boundary conditions at infinite Pr, the logarithmic corrections in the bounds, table 1, are suppressed for brevity. The blue plot is the bound derived in § 4.4, valid up to $E = E_m \sim 41.4487$ and $E_0 = 4.1688$. The bound derived in § 4.5 is shown with a green dashed line. The dashed horizontal line denotes when all heat transport is by conduction and $\mathcal{F}_B = \frac{1}{2}$. In D, we show the bounds for stress-free (top, red) and no-slip (bottom, blue) at zero rotation (Arslan & Rojas 2024).

We restrict our attention to quadratic functionals taking the form

$$\mathcal{V}\{T\} := \left\langle \frac{\beta}{2}|T|^2 - [\tau(z) + z - 1]T \right\rangle, \tag{4.2}$$

that are parametrised by a positive constant $\beta > 0$, referred to as the balance parameter and a piecewise-differentiable function $\tau : [0, 1] \to \mathbb{R}$ with a square-integrable derivative that we call the background temperature field. Here $\tau(z)$ satisfies

$$\tau(0) = 1, \quad \tau(1) = 0. \tag{4.3a,b}$$

Introducing a constant, U, and rearranging, (4.1) can be written as

$$\overline{\langle wT \rangle} \leq U - U + \langle wT \rangle + \frac{\mathrm{d}}{\mathrm{d}t}\mathcal{V}\{T\} \leq U, \tag{4.4}$$

where the final inequality holds given that, $U - \langle wT \rangle - (\mathrm{d}/\mathrm{d}t)\mathcal{V}\{T\} \geq 0$, where we can substitute for the Lie derivative of $\mathcal{V}\{T\}$ by using (2.1c). However, the minimum principle, Lemma 2.1, is necessary to obtain an R-dependent bound on $\overline{\langle wT \rangle}$ that approaches $\frac{1}{2}$ from below as R increases. The condition is enforced with a Lagrange multiplier, $\lambda(z)$, so that the problem statement after computations as outlined in previous work (Arslan *et al.* 2021*b*, 2023) becomes

$$\overline{\langle wT \rangle} \leq \inf_{U,\beta,\tau(z),\lambda(z)} \{U \,|\, \mathcal{S}\{\boldsymbol{u}, T\} \geq 0 \ \ \forall (\boldsymbol{u}, T) \in \mathcal{H}_+\}, \tag{4.5}$$

where

$$\mathcal{H}_+ = \{(\boldsymbol{u}, T) \,|\, \text{horizontally periodic}, \boldsymbol{\nabla} \cdot \boldsymbol{u} = 0, (2.3a), (2.4a), T(\boldsymbol{x}) \geq 0 \text{ a.e. } \boldsymbol{x} \in V\}, \tag{4.6}$$

provided $\lambda(z)$ is a non-decreasing function, and

$$\mathcal{S}\{\boldsymbol{u}, T\} := \langle \beta|\boldsymbol{\nabla} T|^2 + \tau'(z)wT + (\beta z - \tau'(z) + \lambda(z))\partial_z T + \tau(z) + U \rangle - \tfrac{1}{2}. \tag{4.7}$$

Ensuring the positivity of the quadratic terms in (4.7) is referred to as the *spectral constraint* and is defined as

$$\langle \beta|\boldsymbol{\nabla} T|^2 + \tau'(z)wT \rangle \geq 0, \tag{4.8}$$

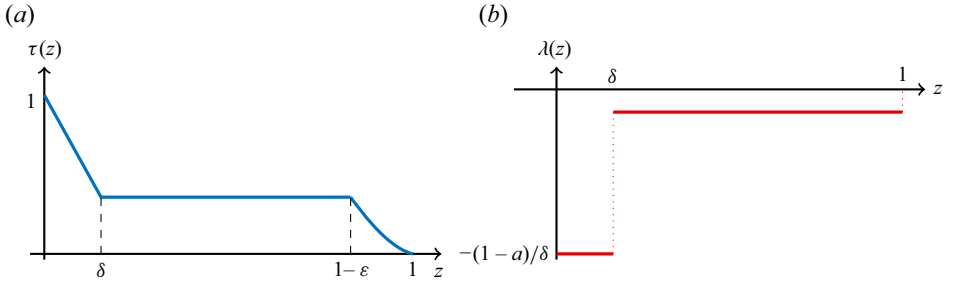

Figure 5. Sketches of the functions $\tau(z)$ in (4.10) and $\lambda(z)$ in (4.11) used to prove (1), where δ is the boundary layer width at the bottom, ε the boundary layer width at the top of the domain and a is (4.12).

where w and T are related by (2.4) and subject to the boundary conditions (2.3). As has been established previously (Arslan *et al.* 2023), provided the spectral constraint is satisfied, then the non-negativity of $\mathcal{S}\{\boldsymbol{u}, T\}$ is ensured when U is given by

$$\overline{\langle wT\rangle} \leq U := \frac{1}{2} + \inf_{\substack{\lambda \in L^2(0,1) \\ \lambda \text{ non-decreasing} \\ \langle\lambda\rangle = -1}} \left\langle \frac{1}{4\beta} \left| \beta\left(z - \frac{1}{2}\right) - \tau'(z) + \lambda(z) \right|^2 - \tau(z) \right\rangle. \tag{4.9}$$

4.2. *Preliminaries*

To establish a bound on $\overline{\langle wT\rangle}$, we state the main choices used in the proof that minimise $U(\beta, \tau, \lambda)$ as defined in (4.9). We make the following choice of background temperature field,

$$\tau(z) := \begin{cases} 1 - \dfrac{1-a}{\delta} z, & 0 \leq z \leq \delta, \\ a, & \delta \leq z \leq 1-\varepsilon, \\ \dfrac{a(1-\varepsilon)}{\varepsilon}\left(\dfrac{1-z}{z}\right), & 1-\varepsilon \leq z \leq 1, \end{cases} \tag{4.10}$$

and set $\lambda(z)$ to be

$$\lambda(z) := \begin{cases} -\dfrac{1-a}{\delta}, & 0 \leq z \leq \delta, \\ -\dfrac{a}{1-\delta}, & \delta \leq z \leq 1. \end{cases} \tag{4.11}$$

The piecewise functions $\tau(z)$ and $\lambda(z)$ are quantified by the boundary layer widths $\delta \in (0, \frac{1}{3})$ and $\varepsilon \in (0, \frac{1}{3})$, where $\delta \leq \varepsilon$, and parameter $a > 0$ that determines the value of $\tau(z)$ in the bulk. See figure 5 for a sketch of the functions.

We further fix

$$a = \tfrac{1}{2}\delta\varepsilon^{1/2}, \tag{4.12}$$

and

$$\beta = \frac{\langle|\tau'(z) - \lambda(z)|^2\rangle^{1/2}}{\langle|z - \frac{1}{2}|^2\rangle^{1/2}}. \tag{4.13}$$

In the following subsections, we prove bounds for different regimes of the Ekman number. We achieve this by using different estimates on the spectral constraint (4.8).

However, the expression for the upper bound on $\overline{\langle wT\rangle}$ in (4.9) remains the same. Therefore, first, we use our choices of $\tau(z)$ in (4.10) and $\lambda(z)$ in (4.11) to estimate (4.9).

4.3. *Estimating the upper bound*

Starting with (4.9) an application of the triangle inequality and the choice of β in (4.13) gives

$$U \leq \frac{1}{2} + \frac{1}{\sqrt{12}}\langle|\tau'(z) - \lambda(z)|^2\rangle^{1/2} - \langle\tau\rangle. \tag{4.14}$$

Then, evaluating the sign positive integral with $\tau(z)$ from (4.10) and $\lambda(z)$ in (4.11), gives

$$\begin{aligned}\langle|\tau'(z) - \lambda(z)|^2\rangle &= \int_\delta^1 |\tau'(z) - \lambda(z)|^2 \,\mathrm{d}z \\ &= \frac{a^2}{(1-\delta)^2}(1-\varepsilon-\delta) + \frac{a^2}{\varepsilon^2}\int_{1-\varepsilon}^1 \left(\frac{1-\varepsilon}{z^2} - \frac{\varepsilon}{1-\delta}\right)^2 \mathrm{d}z. \end{aligned} \tag{4.15}$$

We will require an upper and lower bound on (4.15). Starting with a lower bound, given that $\varepsilon \leq \frac{1}{3}$ and $\delta \leq \frac{1}{3}$, with z in the range $(1-\varepsilon, 1)$, we make the suboptimal but simple estimate that

$$\left(\frac{1-\varepsilon}{z^2} - \frac{\varepsilon}{1-\delta}\right)^2 \geq \frac{1}{9}, \tag{4.16}$$

such that we get

$$\langle|\tau'(z) - \lambda(z)|^2\rangle \geq \frac{a^2}{\varepsilon^2}\int_{1-\varepsilon}^1 \left(\frac{1-\varepsilon}{z^2} - \frac{\varepsilon}{1-\delta}\right)^2 \mathrm{d}z \geq \frac{a^2}{9\varepsilon}. \tag{4.17}$$

For an upper bound on (4.15), given that ε and δ are positive, bounded above by $\frac{1}{3}$ and that $\delta \leq \varepsilon$, we use the estimate $(1-\varepsilon-\delta)(1-\delta)^{-2} \leq \frac{3}{4}\varepsilon^{-1}$ and $z^{-2} \leq (1-\varepsilon)^{-2}$, to obtain

$$\begin{aligned}\langle|\tau'(z) - \lambda(z)|^2\rangle &\leq \frac{3a^2}{4\varepsilon} + \frac{a^2}{\varepsilon^2}\int_{1-\varepsilon}^1 \left(\frac{1-\varepsilon}{z^2} - \frac{\varepsilon}{1-\delta}\right)^2 \mathrm{d}z \\ &\leq \frac{3a^2}{4\varepsilon} + \frac{a^2}{\varepsilon^2}\int_{1-\varepsilon}^1 \frac{1}{(1-\varepsilon)^2} + \frac{\varepsilon^2}{(1-\delta)^2}\,\mathrm{d}z \\ &\leq \frac{3a^2}{4\varepsilon} + \frac{a^2}{\varepsilon}\frac{1+\varepsilon^2}{(1-\varepsilon)^2} \leq \frac{4a^2}{\varepsilon}. \end{aligned} \tag{4.18}$$

Moving on to the integral of $\tau(z)$ in (4.9), we have that

$$\int_0^1 \tau(z)\,\mathrm{d}z = \frac{1}{2}\delta(1-a) - \frac{a}{\varepsilon}(1-\varepsilon)\ln(1-\varepsilon). \tag{4.19}$$

Substituting (4.19) and (4.18) back into (4.14), taking a as given by (4.12) and $\varepsilon, \delta \leq \frac{1}{3}$ such that $\delta^2\varepsilon^{1/2} \leq \frac{\sqrt{3}}{9}\delta$, gives

$$U \leq \tfrac{1}{2} - n\delta - \tfrac{1}{3}\delta\varepsilon^{-1/2}|\ln(1-\varepsilon)|, \tag{4.20}$$

where $n = (18 - 7\sqrt{3})/36$.

4.4. *Large Ekman numbers*

To obtain bounds for large E in this subsection, we use Lemma 2.2. The estimates in Lemma 2.2 are pointwise estimates of the vertical velocity in Fourier space. Therefore, we exploit the horizontal periodicity of $\boldsymbol{u}$ and T and take a Fourier decomposition of w and T in the spectral constraint (4.8). Taking that

$$\begin{bmatrix} T(x,y,z) \\ \boldsymbol{u}(x,y,z) \end{bmatrix} = \sum_{\boldsymbol{k}} \begin{bmatrix} T_{\boldsymbol{k}}(z) \\ \boldsymbol{u}_{\boldsymbol{k}}(z) \end{bmatrix} \mathrm{e}^{\mathrm{i}(k_x x + k_y y)}, \tag{4.21}$$

where the sum is over non-zero wavevectors $\boldsymbol{k} = (k_x, k_y)$ for the horizontal periods L_x and L_y and magnitude of each wavevector is $k = \sqrt{k_x^2 + k_y^2}$. Inserting the Fourier expansions (4.21) into (4.8) gives

$$\int_0^1 \beta |T_{\boldsymbol{k}}'|^2 + \beta k^2 |T_{\boldsymbol{k}}|^2 + \tau'(z) |w_{\boldsymbol{k}} T_{\boldsymbol{k}}| \,\mathrm{d}z \geq 0, \tag{4.22}$$

where the complex conjugate relations of $w_{\boldsymbol{k}} = w_{\boldsymbol{k}}^*$ holds, and $w_{\boldsymbol{k}}$ and $T_{\boldsymbol{k}}$ are subject to the boundary conditions

$$w_{\boldsymbol{k}}(0) = w_{\boldsymbol{k}}(1) = w_{\boldsymbol{k}}'(0) = w_{\boldsymbol{k}}'(1) = 0, \tag{4.23a}$$

$$T_{\boldsymbol{k}}(0) = T_{\boldsymbol{k}}(1) = 0. \tag{4.23b}$$

Based on the boundary conditions, we infer the following two estimates. Given (4.23*a*) applying the fundamental theorem of calculus and Hölders inequality gives

$$|w_{\boldsymbol{k}}| = \int_0^z \int_0^\sigma |\partial_\eta^2 w_{\boldsymbol{k}}(\eta)| \,\mathrm{d}\eta \,\mathrm{d}\sigma \leq \frac{1}{2} z^2 \|w_{\boldsymbol{k}}''\|_\infty, \tag{4.24}$$

and for $T_{\boldsymbol{k}}$, the fundamental theorem of calculus and the Cauchy–Schwarz inequality gives

$$|T_{\boldsymbol{k}}| = \int_0^z |\partial_\eta T_{\boldsymbol{k}}(\eta)| \,\mathrm{d}\eta \leq \sqrt{z} \|T_{\boldsymbol{k}}'\|_2. \tag{4.25}$$

Next, we substitute (4.10) into the sign indefinite term in (4.22) to obtain

$$\int_0^1 \tau'(z) |w_{\boldsymbol{k}} T_{\boldsymbol{k}}| \,\mathrm{d}z = -\frac{1-a}{\delta} \int_0^\delta |w_{\boldsymbol{k}} T_{\boldsymbol{k}}| \,\mathrm{d}z - \frac{a(1-\varepsilon)}{\varepsilon} \int_{1-\varepsilon}^1 z^{-2} |w_{\boldsymbol{k}} T_{\boldsymbol{k}}| \,\mathrm{d}z. \tag{4.26}$$

As Lemma 2.2 contains two estimates for different $\boldsymbol{k}$, we will split the sign indefinite term in half. Then, given that $a \leq 1$, use of (4.24), the Cauchy–Schwarz inequality, (2.7) and (2.8) from Lemma 2.2 gives that

$$\begin{aligned} \frac{1-a}{\delta} \int_0^\delta |w_{\boldsymbol{k}} T_{\boldsymbol{k}}| \,\mathrm{d}z &\leq \frac{1}{2\delta} \int_0^\delta z^{5/2} \,\mathrm{d}z \|T_{\boldsymbol{k}}'\|_2 \|w_{\boldsymbol{k}}''\|_\infty \\ &\leq \frac{\delta^{5/2}}{14} \|T_{\boldsymbol{k}}'\|_2 \|w_{\boldsymbol{k}}''\|_\infty + \frac{\delta^{5/2}}{14} \|T_{\boldsymbol{k}}'\|_2 \|w_{\boldsymbol{k}}''\|_\infty \\ &\leq \frac{c_1}{14} \delta^{5/2} R (1 + \tfrac{1}{4} E^{-2})^{1/4} \|T_{\boldsymbol{k}}'\|_2 \|T_{\boldsymbol{k}}\|_2 \\ &\quad + \frac{c_2}{14} \delta^{5/2} \|T_{\boldsymbol{k}}'\|_2 (R\sqrt{k} \|T_{\boldsymbol{k}}\|_2 + R E^{-1} \|T_{\boldsymbol{k}}\|_2). \end{aligned} \tag{4.27}$$

Taking the term of order $\sqrt{k}$ in (4.27), we estimate further by noting that from (4.25) we have a standard Poincaré inequality of

$$\|T_k\|_2 \leq \frac{1}{\sqrt{2}}\|T_k'\|_2, \tag{4.28}$$

such that the use of Young's inequality twice gives

$$\begin{aligned}\frac{1}{14}\delta^{5/2}R\sqrt{k}c_2\|T_k'\|_2\|T_k\|_2 &\leq \frac{\beta}{2}k\|T_k\|_2\|T_k'\|_2 + \frac{c_2^2}{392\beta}\delta^5R^2\|T_k\|_2\|T_k'\|_2 \\ &\leq \frac{\beta}{2}k^2\|T_k\|_2^2 + \frac{\beta}{8}\|T_k'\|_2^2 + \frac{c_2^2}{392\sqrt{2}\beta}\delta^5R^2\|T_k'\|_2^2. \end{aligned}\tag{4.29}$$

Then, substituting (4.29) into (4.27), the integral at the lower boundary becomes

$$\begin{aligned}\frac{1-a}{\delta}\int_0^\delta |w_kT_k|\,\mathrm{d}z &\leq \frac{\beta}{2}k^2\|T_k\|_2^2 + \frac{\beta}{8}\|T_k'\|_2^2 + \frac{c_2^2}{392\sqrt{2}\beta}\delta^5R^2\|T_k'\|_2^2 \\ &+ \frac{c_1}{14\sqrt{2}}\delta^{5/2}R(1+\tfrac{1}{4}E^{-2})^{1/4}\|T_k'\|_2^2 + \frac{c_2}{14\sqrt{2}}\delta^{5/2}RE^{-1}\|T_k'\|_2^2. \end{aligned}\tag{4.30}$$

We realise that for a sufficiently small Ekman number, the term of order E^{-1} is larger than $(1+E^{-2})^{1/4}$ such that if we make the estimate

$$c_1(1+\tfrac{1}{4}E^{-2})^{1/4} \leq c_2E^{-1}, \tag{4.31}$$

we get a quadratic form in terms of E^2, that places an upper bound on E of

$$E \leq E_m = \frac{1}{2\sqrt{2}}(-1+\sqrt{1+64(c_2^4/c_1^4)})^{1/2} = 41.4487. \tag{4.32}$$

Now, (4.30) becomes

$$\begin{aligned}\frac{1-a}{\delta}\int_0^\delta |w_kT_k|\,\mathrm{d}z &\leq \frac{\beta}{2}k^2\|T_k\|_2^2 + \frac{\beta}{8}\|T_k'\|_2^2 + \frac{c_2^2}{392\sqrt{2}\beta}\delta^5R^2\|T_k'\|_2^2 \\ &+ \frac{c_2}{7\sqrt{2}}\delta^{5/2}RE^{-1}\|T_k'\|_2^2. \end{aligned}\tag{4.33}$$

Returning to the integral at the upper boundary in (4.26), we apply the same procedure, where (4.24) and (4.25) are instead

$$|w_k| \leq \tfrac{1}{2}(1-z)^2\|w_k''\|_\infty, \quad |T_k| \leq \sqrt{1-z}\|T_k'\|_2. \tag{4.34a,b}$$

Given $\varepsilon \leq \frac{1}{3}$ we use that $z^{-2} \leq (1-\varepsilon)^{-2}$ to get

$$\frac{a(1-\varepsilon)}{\varepsilon}\int_{1-\varepsilon}^1 z^{-2}|w_kT_k|\,\mathrm{d}z \leq \frac{a}{\varepsilon(1-\varepsilon)}\int_{1-\varepsilon}^1 |w_kT_k|\,\mathrm{d}z \leq \frac{3a}{2\varepsilon}\int_{1-\varepsilon}^1 |w_kT_k|\,\mathrm{d}z. \tag{4.35}$$

By use of Lemma 2.2, along with (4.34), (4.28), Young's inequality and (4.31), we can estimate the integral at the upper boundary to obtain

$$\begin{aligned}\frac{a(1-\varepsilon)}{\varepsilon}\int_{1-\varepsilon}^1 z^{-2}|w_kT_k|\,\mathrm{d}z &\leq \frac{3a}{2\varepsilon}\int_{1-\varepsilon}^1 |w_kT_k|\,\mathrm{d}z \leq \frac{\beta}{2}k^2\|T_k\|_2^2 + \frac{\beta}{8}\|T_k'\|_2^2 \\ &+ \frac{9c_2^2}{6272\sqrt{2}\beta}\delta^2\varepsilon^6R^2\|T_k'\|_2^2 + \frac{3}{28\sqrt{2}}c_2\delta\varepsilon^3RE^{-1}\|T_k'\|_2^2. \end{aligned}\tag{4.36}$$

Substituting (4.33) and (4.36) back into the spectral constraint (4.22) gives

$$\left(\frac{3\beta}{4}-\frac{c_2^2}{392\sqrt{2}}\frac{\delta^5R^2}{\beta}-\frac{c_2}{7\sqrt{2}}\delta^{5/2}RE^{-1}-\frac{3c_2}{28\sqrt{2}}\delta\varepsilon^3RE^{-1}-\frac{9c_2^2}{6272\sqrt{2}}\frac{\delta^2\varepsilon^6R^2}{\beta}\right)\|T_k'\|_2^2\geq 0. \tag{4.37}$$

The spectral condition is satisfied provided the term in the brackets of (4.37) is non-negative. Note that we have an explicit expression for β in (4.13), which in conjunction with the lower bound in (4.17) gives the following lower bound on β of

$$\beta\geq\frac{\sqrt{3}}{3}\delta. \tag{4.38}$$

After estimating β from below with (4.38) and making the choice

$$\delta=(\tfrac{9}{16})^{1/3}\varepsilon^2, \tag{4.39}$$

the condition for the positivity of (4.37) becomes, after rearranging,

$$1-\frac{c_2^2}{49\sqrt{2}}\delta^3R^2-\frac{8c_2}{7\sqrt{6}}\delta^{3/2}RE^{-1}\geq 0. \tag{4.40}$$

In (4.40), two possible choices of $\delta=\delta(R,E)$ guarantee the non-negativity of the left-hand side. If the second negative term dominates the first, i.e.

$$\frac{c_2^2}{49\sqrt{2}}\delta^3R^2\leq\frac{8\,c_2}{7\sqrt{6}}\delta^{3/2}RE^{-1}, \tag{4.41}$$

then (4.40) becomes

$$\delta\leq\left(\frac{7\sqrt{6}}{16c_2}\right)^{2/3}R^{-2/3}E^{2/3}. \tag{4.42}$$

Taking δ as large as possible in (4.42) and substituting back into (4.40) implies that $E\leq 8(\sqrt{2}/3)^{1/2}$. In the opposite scenario, where

$$\frac{8c_2}{7\sqrt{6}}\delta^{3/2}RE^{-1}\leq\frac{c_2^2}{49\sqrt{2}}\delta^3R^2, \tag{4.43}$$

then (4.40) becomes

$$\delta\leq\left(\frac{49\sqrt{2}}{2c_2^2}\right)^{1/3}R^{-2/3}, \tag{4.44}$$

which holds for $E\geq 8(\sqrt{2}/3)^{1/2}$. In summary, the spectral condition holds if the condition in (4.40) is satisfied and (4.40) is guaranteed when we take δ as large as possible in (4.42)

and (4.44). As a result, we have that

$$\delta = \begin{cases} \left(\dfrac{7\sqrt{6}}{16c_2}\right)^{2/3} R^{-2/3}E^{2/3}, & E \leq 8(\sqrt{2}/3)^{1/2}, \\ \left(\dfrac{49\sqrt{2}}{2c_2^2}\right)^{1/3} R^{-2/3}, & E \geq 8(\sqrt{2}/3)^{1/2}, \end{cases} \tag{4.45}$$

and, by (4.39), that

$$\varepsilon = \begin{cases} \left(\dfrac{7\sqrt{6}}{12c_2}\right)^{1/3} R^{-1/3}E^{1/3}, & E \leq 8(\sqrt{2}/3)^{1/2}, \\ \left(\dfrac{392\sqrt{2}}{9c_2^2}\right)^{1/6} R^{-1/3}, & E \geq 8(\sqrt{2}/3)^{1/2}. \end{cases} \tag{4.46}$$

Therefore, substituting (4.45) and (4.46) back into (4.20), along with the fact that $\overline{\langle wT\rangle} \leq U$ and (1.1) to obtain

$$\mathcal{F}_B \geq \begin{cases} d_1R^{-2/3}E^{2/3} + d_2R^{-1/2}E^{1/2}|\ln(1 - d_3R^{-1/3}E^{1/3})|, & E \leq 8(\sqrt{2}/3)^{1/2}, \\ d_4R^{-2/3} + d_5R^{-1/2}|\ln(1 - d_6R^{-1/3})|, & 8(\sqrt{2}/3)^{1/2} \leq E \leq E_m, \end{cases} \tag{4.47}$$

where the constants d_1 to d_6 are collated in Appendix A. Finally, in § 4.2 we chose that both boundary layer widths are in $(0, \frac{1}{3})$, therefore given (4.45) and (4.46) the bound obtained in (4.47) holds for all $R \geq 0.4715$.

4.5. *Small Ekman numbers*

Next, we demonstrate a proof of the bound on $\mathcal{F}_B$ valid for small E in (1). Here, we use Lemma 2.3 to demonstrate the non-negativity of the spectral constraint (4.8). The estimates used in this subsection do not require estimates in Fourier space.

Starting with the spectral constraint in (4.8), we start by substituting for $\tau(z)$ from (4.10) into the sign-indefinite term and using the estimate $z^{-2} \leq (1-\varepsilon)^{-2}$ at the upper boundary gives

$$\langle \tau'(z)wT\rangle \geq -\frac{1-a}{\delta}\left\langle \int_0^\delta wT\,\mathrm{d}z\right\rangle_h - \frac{a}{\varepsilon}(1-\varepsilon)^{-1}\left\langle \int_{1-\varepsilon}^1 wT\,\mathrm{d}z\right\rangle_h. \tag{4.48}$$

We first consider the integral in (4.48) near $z = 0$ and obtain an estimate on wT. Since we require a lower bound on the right-hand side of (4.48), we can rearrange the order of integration of the first term on the right-hand side of (4.48) and estimate the integral from above. Given the boundary conditions (2.3), use of the fundamental theorem of calculus,

(2.4*b*) and integration by parts gives

$$\langle|wT|\rangle_h = \left\langle\left|\int_0^z \partial_s(wT)\,\mathrm{d}s\right|\right\rangle_h = \left\langle\left|\int_0^z T\partial_s w + w\partial_s T\,\mathrm{d}s\right|\right\rangle_h = \left\langle\left|\int_0^z -ET\nabla^2\zeta + w\partial_s T\,\mathrm{d}s\right|\right\rangle_h$$
$$= E\langle|\zeta' T|\rangle_h + \left\langle\left|\int_0^z E\boldsymbol{\nabla}\zeta\boldsymbol{\nabla}T + w\partial_s T\,\mathrm{d}s\right|\right\rangle_h. \tag{4.49}$$

Then, given the boundary condition on the velocity and temperature in (2.3), we have that

$$|w(\cdot,z)| \leq \frac{2}{3}z^{3/2}\left(\int_0^1 |w''(\cdot,z)|^2\,\mathrm{d}z\right)^{1/2}, \quad \langle T^2\rangle_h^{1/2} \leq \sqrt{z}\langle|\boldsymbol{\nabla}T|^2\rangle^{1/2}, \tag{4.50a,b}$$

use of which, along with multiple applications of the Cauchy–Schwarz inequality in (4.49), and that for $f \in L^2(0,1)$ we have $\langle|f'|^2\rangle_h \leq \langle|\boldsymbol{\nabla}f|^2\rangle_h \leq \langle|\boldsymbol{\nabla}f|^2\rangle$, gives

$$\langle|wT|\rangle_h \leq E\langle|\zeta'|^2\rangle_h^{1/2}\langle|T|^2\rangle_h^{1/2} + E\langle|\boldsymbol{\nabla}\zeta|^2\rangle^{1/2}\langle|\boldsymbol{\nabla}T|^2\rangle^{1/2} + \frac{z^2}{3}\left\langle\int_0^z |\partial_s T|^2\,\mathrm{d}s\right\rangle_h^{1/2}\langle|w''|^2\rangle^{1/2}$$
$$\leq \left((\sqrt{z}+1)E\langle|\boldsymbol{\nabla}\zeta|^2\rangle^{1/2} + \frac{1}{3}z^2\langle|\nabla^2 w|^2\rangle^{1/2}\right)\langle|\boldsymbol{\nabla}T|^2\rangle^{1/2}. \tag{4.51}$$

Next, we use Lemma 2.3, to bound both $\langle|\boldsymbol{\nabla}\zeta|^2\rangle$ and $\langle|\nabla^2 w|^2\rangle$ from above and given that T is horizontally periodic with Dirichlet boundary conditions at $z = 0$ and 1 we have the standard Poincaré inequality $\langle|T|^2\rangle \leq (1/\pi^2)\langle|\boldsymbol{\nabla}T|^2\rangle$, which gives

$$\langle|wT|\rangle_h \leq \left(\frac{ER}{\sqrt{2}\pi}(1+\sqrt{z}) + \frac{1}{3\pi}z^2 R\right)\langle|\boldsymbol{\nabla}T|^2\rangle. \tag{4.52}$$

Then, substituting back into the integral at the boundary, whereby (4.12) we have $1-a \leq 1$, we get that

$$\frac{1-a}{\delta}\int_0^\delta \langle|wT|\rangle_h\,\mathrm{d}z \leq \left(\frac{ER}{\sqrt{2}\pi}\left(1+\frac{2}{3}\delta^{1/2}\right) + \frac{1}{9\pi}\delta^2 R\right)\langle|\boldsymbol{\nabla}T|^2\rangle. \tag{4.53}$$

The same estimates hold at the upper boundary with a given by (4.12) and z replaced by $1-z$. Then, since $\varepsilon \leq \frac{1}{3}$ we can take $1-\varepsilon \leq 1$ to obtain

$$\frac{1}{2}\delta\varepsilon^{-1/2}(1-\varepsilon)^{-1}\int_{1-\varepsilon}^1 \langle|wT|\rangle_h\,\mathrm{d}z \leq \frac{3}{4}\delta\varepsilon^{1/2}\left(\frac{ER}{\sqrt{2}\pi}\left(1+\frac{2}{3}\varepsilon^{1/2}\right) + \frac{1}{9\pi}\varepsilon^2 R\right)\langle|\boldsymbol{\nabla}T|^2\rangle. \tag{4.54}$$

Substituting (4.53) and (4.54) back into (4.48) and then into (4.8), gives after use of the lower bound on β from (4.38) that

$$\left(\frac{\sqrt{3}\delta}{3} - \frac{ER}{\sqrt{2}\pi}\left(1+\frac{2\delta^{1/2}}{3}\right) - \frac{\delta^2 R}{9\pi} - \frac{3\delta\varepsilon^{1/2}ER}{4\sqrt{2}\pi}\left(1+\frac{2\varepsilon^{1/2}}{3}\right) - \frac{\delta\varepsilon^{5/2}R}{12\pi}\right)\langle|\boldsymbol{\nabla}T|^2\rangle \geq 0. \tag{4.55}$$

Since $\varepsilon \leq \frac{1}{3}$ and $\delta \leq \frac{1}{3}$, then, we will make estimates, $1 + 2\delta^{1/2}/3 \leq \sqrt{2}\pi/3$ and $1 + 2\varepsilon^{1/2}/3 \leq \sqrt{2}\pi/3$, such that after rearranging the spectral constraint becomes

$$\sqrt{3}\delta - ER - \frac{\delta^2 R}{3\pi} - \frac{3}{4}\delta\varepsilon^{1/2}ER - \frac{\delta\varepsilon^{5/2}R}{4\pi} \geq 0. \tag{4.56}$$

In (4.56), the first negative term does not contain an explicit δ dependence, and so we will, at the very least, choose that

$$ER \leq \frac{\sqrt{3}}{2}\delta. \tag{4.57}$$

Using (4.57) and further making the choice

$$\delta = \frac{3}{4}\varepsilon^{5/2}, \tag{4.58}$$

gives

$$\frac{\sqrt{3}}{2} - \frac{2}{3\pi}\delta R - \left(\frac{3}{4}\right)^{4/5}\delta^{1/5}ER \geq 0. \tag{4.59}$$

Similar to the proof of a bound for large Ekman numbers in § 4.4, we have a constraint that we consider in two cases. If in (4.59), the second negative term dominates the first such that

$$\frac{2}{3\pi}\delta R \leq \left(\frac{3}{4}\right)^{4/5}\delta^{1/5}ER, \tag{4.60}$$

then

$$\delta \leq \frac{\sqrt{3}}{36}E^{-5}R^{-5}, \tag{4.61}$$

however, if this δ is to satisfy the spectral constraint then its implication on (4.57) and (4.59) need to be checked. If we take δ to be as large as possible in (4.61), then, up to constants, we get from (4.57) and (4.59) that

$$E \gtrsim R^{-4/5} \quad \text{and} \quad E \lesssim R^{-1}, \tag{4.62a,b}$$

which leads to a contradiction, and the initial assumption cannot be true. Assuming, instead, that

$$\left(\frac{3}{4}\right)^{4/5}\delta^{1/5}ER \leq \frac{2}{3\pi}\delta R, \tag{4.63}$$

gives in (4.59) that

$$\delta \leq \frac{3\sqrt{3}\pi}{8}R^{-1}. \tag{4.64}$$

Taking δ as large as possible in (4.64), the constraints from (4.57) implies that

$$E \leq \frac{9\pi}{16}R^{-2}, \tag{4.65}$$

Finally, substituting the largest δ from (4.64) into (4.58) gives

$$\varepsilon = \left(\frac{\sqrt{3}\pi}{2}\right)^{2/5}R^{-2/5}. \tag{4.66}$$

Then, taking δ as large as possible in (4.64), (4.66), substituting into (4.20), along with the fact that $\overline{\langle wT\rangle} \leq U$ and (1.1) we get that

$$\mathcal{F}_B \geq d_7R^{-1} + d_8R^{-4/5}|\ln(1 - d_9R^{-2/5})|, \quad E \leq \frac{9\pi}{16}R^{-2}, \tag{4.67a,b}$$

where the constants d_7 to d_9 are collated in Appendix A. Finally, for completeness, we verify that the choice of $\varepsilon, \delta \in (0, \frac{1}{3})$ made in § 4.2 is not restrictive. Since δ is smaller

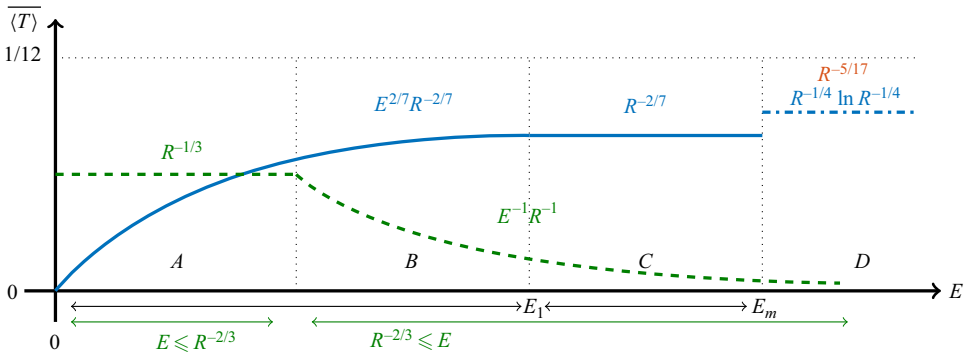

Figure 6. Illustration of the lower bounds on the mean temperature between no-slip and isothermal boundary conditions at infinite Pr. The blue plot is the bound derived in § 5.3, valid up to $E_m \sim 41.4487$ and $E_1 = 8$. The bounds derived in § 5.4 are shown with a green plot. The dashed horizontal line denotes when all heat transport is by conduction and $\overline{\langle T\rangle} = \frac{1}{12}$. In D, we show the previously known best bound for stress-free (top, red) (Whitehead & Doering 2012) and no-slip (bottom, blue) (Whitehead & Doering 2011*a*) at zero rotation.

than ε as expressed in (4.58), taking δ as large as possible in (4.64) the bound obtained in (4.67) holds for all $R \geq 6.1216$.

5. Bounds on the mean temperature

In this section, we prove bounds on $\overline{\langle T\rangle}$ with the auxiliary functional method by using the same strategy as in § 4.1. First, we derive a variational problem for obtaining a lower bound on $\overline{\langle T\rangle}$, with a different quadratic auxiliary functional to (4.2). Then, given our choice of background profile $\varphi(z)$, we can estimate the lower bound L on $\overline{\langle T\rangle}$ in terms of the parameters of $\varphi(z)$. We then prove bounds for large and small E numbers by Lemmas 2.2 and 2.3. The proofs in this section are algebraically lighter than the proof for a bound on $\overline{\langle wT\rangle}$, primarily due to two reasons. The first is that the minimum principle on T, Lemma 2.1, is not required, and the second, the balance parameters do not have a R dependence. The lower bounds we prove on $\overline{\langle T\rangle}$, including those already known, are illustrated in figure 6.

5.1. *The auxiliary functional method*

By the auxiliary functional method, we obtain an explicit variational problem that we solve to obtain a bound on $\overline{\langle T\rangle}$. The following derivation, albeit in the language of the classic background field method approach, appears in previous papers (Whitehead & Doering 2011*a*, 2012). Here, we only present an outline within the auxiliary functional framework.

Starting with the quadratic auxiliary functional

$$\mathcal{V}\{T\} = \langle -\tfrac{1}{2}|T|^2 + 2\varphi(z)T\rangle, \tag{5.1}$$

where $\varphi(z)$ is the background temperature field subject to the boundary conditions

$$\varphi(0) = \varphi(1) = 0. \tag{5.2}$$

Then, provided $\mathcal{V}\{T(t)\}$ is bounded along solutions of (2.1), the time derivative of the long-time average of $\mathcal{V}\{T\}$ is zero, such that we can write

$$\overline{\langle T\rangle} = L - \left(L - \overline{\langle T\rangle + \frac{\mathrm{d}}{\mathrm{d}t}\mathcal{V}\{T\}}\right) \geq L, \tag{5.3}$$

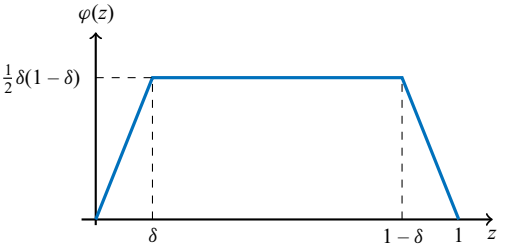

Figure 7. Sketches of the functions $\varphi(z)$ in (5.8) used to prove (1), where δ is the boundary layer widths.

where the inequality comes from assuming that, $L - \overline{\langle T\rangle + (\mathrm{d}/\mathrm{d}t)\mathcal{V}\{T\}} \leq L - \langle T\rangle - (\mathrm{d}/\mathrm{d}t)\mathcal{V}\{T\} \leq 0$. Noting that we again bound the terms in the long-time integral by the pointwise in time maximum over all periodic $\boldsymbol{u}$ and T, where $\boldsymbol{\nabla}\cdot\boldsymbol{u} = 0$, subject to the boundary conditions (2.3). Hence, after substituting for the Lie derivative of $\mathcal{V}\{T\}$ by use of (2.1*c*) and rearranging, we have, after appropriate manipulations, the following variational problem

$$\overline{\langle T\rangle} \geq \inf_{L,\varphi(z)} \{L \,|\, \mathcal{S}\{\boldsymbol{u}, T\} \geq 0 \;\; \forall (\boldsymbol{u}, T) \in \mathcal{H}_+\}, \tag{5.4}$$

where

$$\mathcal{S}\{\boldsymbol{u}, T\} := \langle |\boldsymbol{\nabla} T|^2 + \varphi'(z) w T - \varphi'(z)\partial_z T + \varphi(z) - L\rangle. \tag{5.5}$$

In this case, the spectral constraint is given by

$$\langle |\boldsymbol{\nabla} T|^2 + 2\varphi'(z) w T\rangle \geq 0. \tag{5.6}$$

Then, by optimising the linear terms in (5.5) the explicit expression for L is given

$$L := 2\langle \varphi(z)\rangle - \langle |\varphi'(z)|^2\rangle. \tag{5.7}$$

5.2. *Preliminaries*

To establish a lower bound on $\overline{\langle T\rangle}$, we take the following class of background fields

$$\varphi(z) := \begin{cases} \frac{1}{2}(1-\delta)z, & 0 \leq z \leq \delta, \\ \frac{1}{2}\delta(1-\delta), & \delta \leq z \leq 1-\delta, \\ \frac{1}{2}(1-\delta)(1-z), & 1-\delta \leq z \leq 1. \end{cases} \tag{5.8}$$

The background field is determined entirely by $\delta \in (0, \frac{1}{3})$, the width of the boundary layers at the top and bottom of the domain, sketched in figure 7. In contrast to § 4, no advantage follows from background fields with boundary layers of different widths.

The lower bounds on $\overline{\langle T\rangle}$ for different Ekman numbers rely on different estimates of the velocity in the spectral constraint (5.6) given the diagnostic (2.4). Given the choice of background profile (5.8), the expression for the lower bound $L = L(\delta)$ is unchanged based on the estimates we use to demonstrate the non-negativity of the spectral constraint for different Ekman numbers. Thus, we now estimate L in (5.7) given (5.8). Substituting for $\varphi(z)$ from (5.8), we get

$$L = \tfrac{1}{2}\delta(1-\delta)^2. \tag{5.9}$$

Since $\delta \leq \frac{1}{3}$, then the estimate $1 - \delta \geq \frac{2}{3}$, gives

$$L \geq \tfrac{2}{9}\delta. \tag{5.10}$$

5.3. *Large Ekman numbers*

We can now proceed to establish a lower bound on $\overline{\langle T \rangle}$ by establishing the conditions under which the spectral constraint of (5.4) is satisfied, given the choice of background temperature field (5.8) and by use of Lemma 2.2. The estimates in Lemma 2.2 apply to (2.4) in Fourier space so we exploit horizontal periodicity and substitute (4.21) into (5.6) such that the spectral constraint in Fourier space is

$$\int_0^1 |T_k'|^2 + k^2|T_k|^2 + 2\varphi'(z)\,\mathrm{Re}\{w_k T_k^*\}\,\mathrm{d}z \geq 0. \tag{5.11}$$

Substituting for $\varphi(z)$ and using the fact that $\delta \leq \frac{1}{3}$ gives $-(1-\delta) \geq -1$, the sign-indefinite of (5.11) is

$$\begin{aligned} 2\int_0^1 \varphi'(z)\,\mathrm{Re}\{w_k T_k^*\}\,\mathrm{d}z &\geq -2\int_0^1 |\varphi'(z) w_k T_k|\,\mathrm{d}z \\ &\geq -\int_0^\delta |w_k T_k|\,\mathrm{d}z - \int_{1-\delta}^1 |w_k T_k|\,\mathrm{d}z. \end{aligned} \tag{5.12}$$

Due to the symmetry in the boundary conditions and $\varphi(z)$, we only demonstrate estimates on the integral at the lower boundary since that at the top gives an identical contribution. Using the estimates of (4.24) and (4.25) on w_k and T_k, Lemma 2.2 and Young's inequality, we get

$$\begin{aligned} \int_0^\delta |w_k T_k|\,\mathrm{d}z &\leq \frac{1}{2}\int_0^\delta z^{5/2}\,\mathrm{d}z \|T_k'\|_2 \|w_k''\|_\infty \\ &= \frac{1}{14}\delta^{7/2}\|T_k'\|_2\|w_k''\|_\infty + \frac{1}{14}\delta^{7/2}\|T_k'\|_2\|w_k''\|_\infty \\ &\leq \frac{\delta^{7/2}}{14} c_1 R(1+\tfrac{1}{4}E^{-2})^{1/4}\|T_k'\|_2\|T_k\|_2 \\ &\quad + \frac{\delta^{7/2}}{14}\|T_k'\|_2 c_2 (R\sqrt{k}\|T_k\|_2 + RE^{-1}\|T_k\|_2). \end{aligned} \tag{5.13}$$

Taking the term of order $\sqrt{k}$, estimating by use of Young's inequality twice and (4.28) gives

$$\begin{aligned} \frac{1}{14}\delta^{7/2} R\sqrt{k} c_2 \|T_k'\|_2\|T_k\|_2 &\leq \frac{\sqrt{2}}{2} k\|T_k\|_2\|T_k'\|_2 + \frac{c_2^2}{392\sqrt{2}}\delta^7 R^2\|T_k\|_2\|T_k'\|_2 \\ &\leq \frac{1}{2}k^2\|T_k\|_2^2 + \frac{1}{4}\|T_k'\|_2^2 + \frac{c_2^2}{784}\delta^7 R^2\|T_k'\|_2^2. \end{aligned} \tag{5.14}$$

Therefore, the integral from 0 to δ simplifies to

$$\begin{aligned} \int_0^\delta |w_k T_k|\,\mathrm{d}z &\leq \frac{1}{2}k^2\|T_k\|_2^2 + \frac{1}{4}\|T_k'\|_2^2 + \frac{c_2^2}{784}\delta^7 R^2\|T_k'\|_2^2 \\ &\quad + \frac{\sqrt{2}}{28} c_1 \delta^{7/2} R(1+\tfrac{1}{4}E^{-2})^{1/4}\|T_k'\|_2^2 + \frac{\sqrt{2}}{28} c_2 \delta^{7/2} RE^{-1}\|T_k'\|_2^2. \end{aligned} \tag{5.15}$$

By equivalent estimates at the upper boundary, we get the same upper bound such that (5.12) becomes

$$2\int_0^1 \varphi'(z)\,\mathrm{Re}\{w_{\boldsymbol{k}}T_{\boldsymbol{k}}^*\}\,\mathrm{d}z \geq -k^2\|T_{\boldsymbol{k}}\|_2^2 - \frac{1}{2}\|T_{\boldsymbol{k}}'\|_2^2 - \left(\frac{c_2^2}{392}\delta^7R^2 + \frac{\sqrt{2}}{14}c_1\delta^{7/2}R(1+\tfrac{1}{4}E^{-2})^{1/4} + \frac{\sqrt{2}}{14}c_2\delta^{7/2}RE^{-1}\right)\|T_{\boldsymbol{k}}'\|_2^2. \tag{5.16}$$

Finally, we use the estimate in (4.31), which places an upper limit on $E = E_m$ in (4.32), for which the bounds are valid. Then, substituting (5.16) into (5.11) with (4.31), the spectral constraint becomes

$$\frac{1}{2} - \frac{c_2^2}{392}\delta^7R^2 - \frac{\sqrt{2}}{7}c_2\delta^{7/2}RE^{-1} \geq 0. \tag{5.17}$$

In (5.17), two possible choices of $\delta = \delta(R, E)$ guarantee the non-negativity of the left-hand side. If

$$\frac{c_2^2}{392}\delta^7R^2 \leq \frac{\sqrt{2}}{7}c_2\delta^{7/2}RE^{-1}, \tag{5.18}$$

then from (5.17) we have that

$$\delta \leq \left(\frac{7\sqrt{2}}{8c_2}\right)^{2/7} R^{-2/7}E^{2/7}. \tag{5.19}$$

Taking (5.19) as large as possible, substituting back into (5.17) and rearranging, we find that the spectral constraint holds when $E \leq 8$. In the opposite scenario, where

$$\frac{\sqrt{2}}{7}c_2\delta^{7/2}RE^{-1} \leq \frac{c_2^2}{392}\delta^7R^2, \tag{5.20}$$

substituted back into (5.17) gives that

$$\delta \leq \left(\frac{196}{c_2^2}\right)^{1/7} R^{-2/7}, \tag{5.21}$$

which holds for $E \geq 8$. In summary, we have that

$$\delta = \begin{cases} \left(\dfrac{7\sqrt{2}}{8c_2}\right)^{2/7} R^{-2/7}E^{2/7}, & E \leq 8, \\ \left(\dfrac{196}{c_2^2}\right)^{1/7} R^{-2/7}, & E \geq 8, \end{cases} \tag{5.22}$$

which we can finally substitute into (5.10) remembering that $\overline{\langle T\rangle} \geq L$ to obtain that

$$\overline{\langle T\rangle} \geq \begin{cases} d_{10}R^{-2/7}E^{2/7}, & E \leq 8, \\ d_{11}R^{-2/7}, & 8 \leq E \leq E_m, \end{cases} \tag{5.23}$$

where d_{10} and d_{11} are given in Appendix A. A final check is on the validity of the bounds given choices made in § 5.2 that δ is in $(0, \frac{1}{3})$. Given (5.22) the bound obtained in (5.23) holds for all $R \geq 7.1363$ when $E \leq 8$ and $R \geq 10.0922$ when $E \geq 8$.

5.4. *Small Ekman numbers*

Next, we move on to the proof of the lower bound on $\overline{\langle T\rangle}$ in (1) valid for a small E. Here, we use Lemma 2.3, which does not require estimates in Fourier space. Starting with the spectral constraint (5.6) and substituting for $\varphi(z)$ from (5.8), the sign-indefinite term becomes

$$2\langle\varphi'(z)wT\rangle \geq -2\langle|\varphi'(z)wT|\rangle \geq -\left\langle\int_0^\delta |wT|\,\mathrm{d}z\right\rangle_h - \left\langle\int_{1-\delta}^1 |wT|\,\mathrm{d}z\right\rangle_h. \tag{5.24}$$

In § 4.5, we established the estimate (4.52) and can substitute directly into the integral at the lower boundary in (5.24) to obtain

$$\left\langle\int_0^\delta |wT|\,\mathrm{d}z\right\rangle_h \leq \left[\frac{ER}{\sqrt{2}\pi}\left(\delta+\frac{2\delta^{3/2}}{3}\right)+\frac{1}{9\pi}\delta^3R\right]\langle|\boldsymbol{\nabla}T|^2\rangle. \tag{5.25}$$

The integral at the upper boundary gives an identical estimate such that the spectral constraint of (5.6) becomes

$$\begin{aligned}\langle|\boldsymbol{\nabla}T|^2+2\varphi'(z)wT\rangle &\geq \langle|\boldsymbol{\nabla}T|^2-2|\varphi'(z)wT|\rangle\\ &\geq \langle|\boldsymbol{\nabla}T|^2\rangle-2\left[\frac{ER}{\sqrt{2}\pi}\left(\delta+\frac{2\delta^{3/2}}{3}\right)+\frac{1}{9\pi}\delta^3R\right]\langle|\boldsymbol{\nabla}T|^2\rangle \geq 0.\end{aligned} \tag{5.26}$$

Therefore, the spectral constraint becomes the condition

$$1-\frac{2ER}{\sqrt{2}\pi}\left(\delta+\frac{2\delta^{3/2}}{3}\right)-\frac{1}{9\pi}\delta^3R \geq 0. \tag{5.27}$$

Given that $\delta \leq \frac{1}{3}$, we use the estimate that $1+2\delta^{1/2}/3 \leq \frac{\sqrt{2}\pi}{3}$ to obtain the condition

$$1-\frac{2}{3}ER\delta-\frac{1}{9\pi}\delta^3R \geq 0. \tag{5.28}$$

Once more, the condition admits $\delta=\delta(R,E)$ valid for two cases. If we take

$$\frac{2}{3}ER\delta \leq \frac{1}{9\pi}\delta^3R, \tag{5.29}$$

then (5.28) is non-negative if

$$\delta \leq \left(\frac{9\pi}{2}\right)^{1/3}R^{-1/3}, \tag{5.30}$$

where when taking δ as large as possible the choice holds when $E \leq \frac{3}{4}(2/9\pi)^{1/3}R^{-2/3}$. In the case where

$$\frac{1}{9\pi}\delta^3R \leq \frac{2}{3}ER\delta, \tag{5.31}$$

then

$$\delta \leq \tfrac{3}{4}R^{-1}E^{-1}, \tag{5.32}$$

for all $E \geq \frac{3}{4}(2/9\pi)^{1/3}R^{-2/3}$. Therefore, the spectral constraint is satisfied if

$$\delta = \begin{cases} \left(\dfrac{9\pi}{8}\right)^{1/3} R^{-1/3}, & E \leq \dfrac{3}{4}\left(\dfrac{2}{9\pi}\right)^{1/3} R^{-2/3}, \\ \dfrac{3}{4}R^{-1}E^{-1}, & E \geq \dfrac{3}{4}\left(\dfrac{2}{9\pi}\right)^{1/3} R^{-2/3}. \end{cases} \tag{5.33}$$

Substituting into (5.10) and remembering further that $\overline{\langle T\rangle} \geq L$, gives

$$\overline{\langle T\rangle} \geq \begin{cases} d_{12}R^{-1/3}, & E \leq \dfrac{3}{4}\left(\dfrac{2}{9\pi}\right)^{1/3} R^{-2/3}, \\ d_{13}R^{-1}E^{-1}, & E \geq \dfrac{3}{4}\left(\dfrac{2}{9\pi}\right)^{1/3} R^{-2/3}, \end{cases} \tag{5.34}$$

where d_{12} and d_{13} are in Appendix A. Finally, for completeness, we verify that the choice of $\delta \in (0, \frac{1}{3})$ made in § 5.2 is not restrictive. Given (5.33) the bound obtained in (5.34) holds for all $R \geq 95.4259$ when $E \leq \frac{3}{4}(2/9\pi)^{1/3}R^{-2/3}$ and for all $R \geq 1$ otherwise.

6. Discussion

6.1. *Regions of validity of the bounds*

Owing to the use of two different estimates (Lemmas 2.2 and 2.3), we need to consider which bounds dominate in the various regions created by the constraints on the bounds. To this effect, first, we plot the regions in which the bounds on $\mathcal{F}_B$ and $\overline{\langle T\rangle}$ overlap in figure 8. For ease of understanding, we split the space of E and R into four main regions. Region I, where R and E are large, corresponds to a slowly rotating buoyancy-dominated flow. Region II is the solid body rotation of the fluid since R and E are small. Region III, where R is large and E small, contains a transition from buoyancy- to rotation-dominated convection provided $R > R_L$ where R_L is the Rayleigh number above which the flow is linearly unstable. At the same time, region IV, where E is small but R cannot get too large, is for rotation-dominated flows.

In figure 8(a), the blue solid line shows $E = 1.7671\,R^{-2}$, the red line is the constant $E_0 = 5.4927$, whereas in figure 8(b) the blue line shows $E = 0.3102R^{-2/3}$, the purple line $E = 1.9273R^{-5/9}$ and the red line is the constant $E_1 = 8$. In both (a) and (b), the yellow line is the constant $E_m = 41.4487$ from (4.32), the dotted vertical line, 26926.6 and the dashed green line is the asymptotic result of (3.15).

Starting with figure 8(a), the bounds of (4.47) and (4.67) split the diagram into four and we evaluate the best bound in each region. For region I, where $E \gtrsim R^{-2}$ and $E_m \geq E \geq E_0$, the only valid bound is $d_4R^{-2/3} + d_5R^{-1/2}|\ln(1 - d_6R^{-1/3})|$. The scaling of the slowly rotating convection bound matches the zero rotation bound of Arslan & Rojas (2024), noting that the initial assumptions on δ and ε can be adjusted such that the constants in the two bounds match. The question of a bound dependent on E that, in the limit of $E \to \infty$, matches the scaling of $R^{-2/3}$ remains open. In region II, $E \lesssim R^{-2}$ and $E_m \geq E \geq E_0$, the best bound would match region I, but the region is below R_L when $E = \infty$, so no convection occurs, and $\mathcal{F}_B = \frac{1}{2}$. In region III, $E \gtrsim R^{-2}$ and $E \leq E_0$, the only bound is $d_1R^{-2/3}E^{2/3} + d_2R^{-1/2}E^{1/2}|\ln(1 - d_3R^{-1/3}E^{1/3})|$, provided $R > R_L$. Finally, in region IV, where $E \lesssim R^{-2}$ and $E \leq E_0$, the best bound is $d_7R^{-1} + d_8R^{-4/5}|\ln(1 - d_9R^{-2/5})|$ again provided that $R > R_L$. While region IV is below the dotted green line in figure 8,

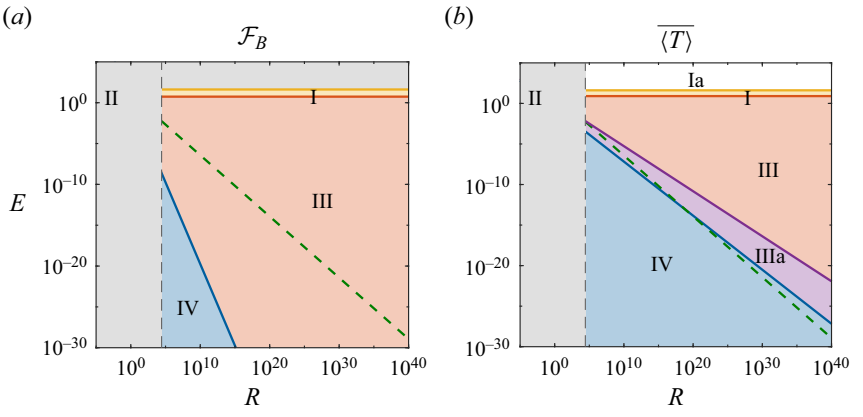

Figure 8. The Rayleigh and Ekman number diagrams for the bounds (4.47), (4.67), (5.23) and (5.34). Grey areas denote regions where the bounds proven in this work do not hold. We plot the regions of validity for the bounds on $\mathcal{F}_B$ in (a) and for $\overline{\langle T \rangle}$ in (b). The blue solid lines correspond to $E = 1.7671\,R^{-2}$ in (a) and $E = 0.3102\,R^{-2/3}$ in (b), with the blue area denoting region IV. The horizontal red solid lines are $E_0 = 5.4927$ in (a) and $E_1 = 8$ in (b) and the red area is region III, where for (b) IIIa is the purple zone with the solid purple line corresponding to $E = 1.9273\,R^{-5/9}$. In both figures, the horizontal yellow lines are $E_m = 41.4487$ with the yellow zone corresponding to region I. The vertical dashed lines are $R_L = 26926.6$ and the green dashed lines are the asymptotic result of (3.15). The four main regions are labelled I to IV.

(3.15) is an asymptotic result for instability with stress-free boundaries. The bounds, on the other hand, are for no-slip boundaries.

We now move on to figure 8(b) and the bounds (5.23) and (5.34). The first difference with (a) is that region I, is split into two. In region I where $E \gtrsim R^{-2/3}$ and $E_m \geq E \geq E_1$, there are two bounds of $d_{13}R^{-1}E^{-1}$ and $d_{11}R^{-2/7}$, where from a comparison of the two the better bound is $d_{11}R^{-2/7}$, due to the requirement of $E \gtrsim R^{-2/3}$. However, for region Ia where $E \gtrsim R^{-2/3}$ and $E \geq E_m$, the only valid bound is $d_{13}R^{-1}E^{-1}$. Region II, where $E \lesssim R^{-2/3}$ and $E \geq E_1$, is below the linear stability limit, so $\overline{\langle T \rangle} = \frac{1}{12}$. In region III, $E \gtrsim R^{-2/3}$ and $E \leq E_1$, there are two bounds of $d_{10}R^{-2/7}E^{2/7}$ and $d_{13}R^{-1}E^{-1}$, and both are valid in different cases. When $R^{-2/3} \lesssim E \lesssim R^{-5/9}$, referred to as region IIIa and shown with the purple region, the better lower bound is $d_{13}R^{-1}E^{-1}$, provided $R > R_L$. If instead $E \gtrsim R^{-5/9}$, then instead the mean temperature is bounded by $d_{10}R^{-2/7}E^{2/7}$. The dashed green line scales as $R^{-3/4}$, so, for sufficiently large R, the entirety of region III corresponds to convecting flows. In region IV, $E \lesssim R^{-2/3}$ and $E \leq E_1$, there are two bounds but the better one is $d_{12}R^{-1/3}$, provided $R > R_L$. Table 1 summarises the above discussion of the results.

Having established the regions where each of the bounds is valid in the E–R space, we now consider the implications of these bounds on rotation in turbulent convection driven by internal heating. Figure 9 compares the bounds proven in this paper with the best-known bounds for IHC without rotation (Whitehead & Doering 2011*a*; Arslan & Rojas 2024). We fix E at 1×10^{-16} and plot the bounds as a function of R, and then fix R at 1×10^{8} and plot them as a function of E. Equivalent to taking horizontal and vertical slices of figure 8 to visualise the bounds along each line segment.

Discontinuities at the intersections in figure 9, defined by the regions of validity for each bound (table 1), are expected and arise from comparing bounds obtained by different lemmas and are a product of the method used to ensure positivity of the spectral constraint of (4.8) in §§ 4 and 5. In addition, across all subplots, the ratio of the bounds

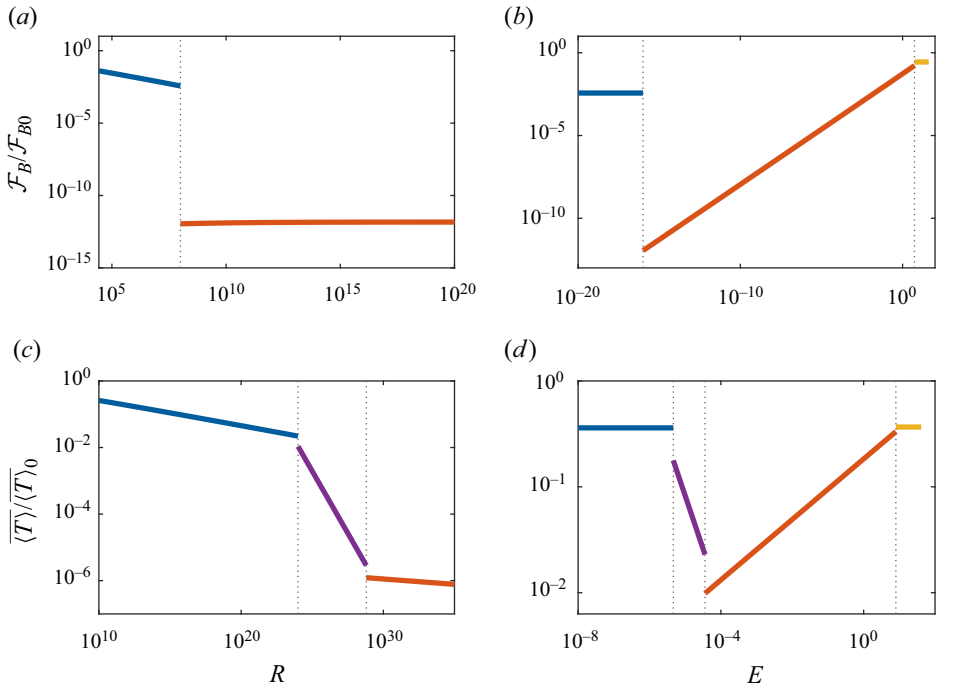

Figure 9. Plots of the ratio of lower bounds on $\mathcal{F}_B$ and $\overline{\langle T\rangle}$ relative to the best-known bounds at zero rotation $\mathcal{F}_{B0}$ and $\overline{\langle T\rangle}_0$ (Whitehead & Doering 2011*a*; Arslan & Rojas 2024), for $E = 1 \times 10^{-16}$ in (*a*) and (*c*) and $R = 1 \times 10^8$ in (*b*) and (*d*). In all of the subplots, the blue lines are the lower bounds in region IV, the red lines are the bounds in region III and the yellow lines are the bounds in Region I, while purple lines in (*c*) and (*d*) are the bounds valid in regions Ia and IIIa for $\overline{\langle T\rangle}$. The bounds themselves are in table 1. Vertical dotted lines show the intersections of the regions for each bound.

is consistently less than 1, though by restricting the choices of δ, ε, and estimates in the proofs, the y values in figure 9 can be made larger. For brevity in the proofs, constants were not optimised. Starting with $\mathcal{F}_B$ at $E = 10^{-16}$, the bounds in region III (red line) have the same scaling as the zero-rotation case, while in region IV (blue line), the bounds decrease, suggesting that at higher R, less heat may escape the domain compared with the non-rotating case. For fixed R, only the bound in region III changes with E: for smaller E, the bound on $\mathcal{F}_B$ is smaller than $\mathcal{F}_{B0}$. For $\overline{\langle T\rangle}$, with E fixed, the bounds scale such that the ratio $\overline{\langle T\rangle}/\overline{\langle T\rangle}_0$ always decreases. However, when R is constant, the scaling in regions IV and I (yellow line) is independent of E. As rotation increases, the ratio decreases in region III but increases in regions Ia and IIIa (purple lines). A smaller lower bound in the rotating case implies a larger possible range for $\mathcal{F}_B$ and $\overline{\langle T\rangle}$. Since rotation introduces new flow regimes, it is possible that some flows cause both quantities to be lower than in the absence of rotation.

Finally, consider the possible heuristic scalings of $\overline{\langle T\rangle} \sim R^{-3/5}E^{-4/5}$ from (B3*b*) and $\mathcal{F}_B \sim R^{-3/10}E^{-2/5}$ from (B4*b*), that may hold for rotation-dominated convection. In the scaling laws, if we fix R and take $E \to 0$, we tend to the uniform upper bounds for both quantities. The lower bounds closest to the heuristic scaling are those in region III (table 1). It is insightful to consider the small E limit where $E \sim R_L^{-3/4}$, and we can write that

$$\overline{\langle T\rangle} \sim \left(\frac{R}{R_L}\right)^{-3/5}, \tag{6.1a}$$

and

$$\mathcal{F}_B \sim \left(\frac{R}{R_L}\right)^{-3/10}, \tag{6.1b}$$

whereas the rigorous bounds in region III (table 1) become

$$\overline{\langle T\rangle} \gtrsim \left(\frac{R}{R_L}\right)^{3/14} R^{-1/2}, \tag{6.2a}$$

and

$$\mathcal{F}_B \gtrsim \left(\frac{R}{R_L}\right)^{1/2} R^{-7/6} + \left(\frac{R}{R_L}\right)^{3/8} R^{-7/8} \left|\ln\left(1 - \left(\frac{R}{R_L}\right)^{1/4} R^{-7/12}\right)\right|. \tag{6.2b}$$

Since R is always a multiple of R_L, for $R > R_L$, the bounds in (6.2), as expected, are smaller than the heuristic scaling laws (6.1). If the lower bounds are not sharp, then this would motivate the question of how to improve the bounds, which we now discuss with concluding remarks.

6.2. *Conclusions*

In this work we prove the first lower bounds on the mean temperature $\overline{\langle T\rangle}$, ((5.23) and (5.34)) and the mean heat flux out of the bottom boundary $\mathcal{F}_B$ ((4.47) and (4.67)), for rotating uniform IHC in the limit of infinite Prandtl number. Using the fact that the momentum equation in RBC and IHC is identical, we adapt estimates from Yan (2004) and Constantin *et al.* (1999) to prove the first Rayleigh- and Ekman-number-dependent bounds on $\overline{\langle T\rangle}$ and $\mathcal{F}_B$ in IHC. By application of the auxiliary functional method, we prove bounds that apply to different regions of buoyancy to rotation-dominated flows, summarised in figure 8 and table 1. In addition to rigorous bounds, we demonstrate that the critical Rayleigh number for linear stability, R_L, asymptotically scales with the Ekman number as $E^{-4/3}$ when the marginally stable states are steady.

In contrast to previous applications of the background field method, there are several unique features in the proofs of bounds in this work. First, the background temperature fields have boundary layers of different widths for the proofs on $\mathcal{F}_B$, but not for $\overline{\langle T\rangle}$. In particular, when we use Lemma 2.2 we find that $\delta = \varepsilon^2$, while when using Lemma 2.3, $\delta = \varepsilon^{5/2}$. The relation from using Lemma 2.2 (§ 4.4) matches the predictions of heuristic arguments (Appendix B). However, whether or not the background profiles are optimal remains unknown and can be addressed with numerical optimisation over a finite range of parameters (Fantuzzi & Wynn 2016; Fantuzzi 2018; Fantuzzi *et al.* 2022). The scaling of the bound obtained for $\mathcal{F}_B$ in the slowly rotating region (region I in figure 8 and table 1) matches the best known bound for zero rotation, however, the constants differ. The scaling of the bounds on $\overline{\langle T\rangle}$ do not match the zero rotation case, but the bounds in this work only hold up to $E \leq E_m = 41.4487$, and the background profile is not logarithmic, which is critical to the bound of Whitehead & Doering (2011*a*). It would be interesting if further investigations can prove a bound that holds for large E too and matches the scaling of the zero rotation bounds on $\overline{\langle T\rangle}$ (Whitehead & Doering 2011*a*) and $\mathcal{F}_B$ (Arslan & Rojas 2024) when $E \to \infty$. The two lemmas used in this work give different bounds for different regions of the E–R parameter. While both estimate the second derivative of the vertical velocity, the estimates hold for different L^p norms with Lemma 2.2 utilising

a finer spectral analysis of the Greens function of (2.1*b*). More generally, Lemma 2.2 is a pointwise estimate in z, and Lemma 2.3 is an integral estimate over the whole domain.

Although rigorous demonstrations of the validity of the results at arbitrary Pr are not provided here, previous work in Tilgner (2022) outlines a strategy for extending bounds from $Pr = \infty$ to finite Pr for RBC. The author achieves this under specific restrictions on E and a numerical approximation of a Greens' function, making the bound semi-analytic. A similar approach appears in Wang & Whitehead (2013) to extend bounds on RBC for stress-free boundaries from infinite Pr to arbitrary Pr in three dimensions (the proof in two dimensions being given in Whitehead & Doering 2011*b*). The barrier to adapting to IHC is the lack of a maximum principle on the temperature of the form $\|T\|_\infty \leq c$, where $c = 1$ for RBC. Proof of any maximum principle for IHC is unknown for any L^p space. Therefore, at best, we can conjecture that akin to RBC, to highest order, the bounds in this work should hold for arbitrary Pr.

In considering turbulent convection subject to rotation, a question of interest is the behaviour in the limit of rapidly rotating convection. Rapidly rotating IHC could be investigated by taking the approach of the nhQG approximation (Julien *et al.* 1996; Sprague *et al.* 2006; Julien *et al.* 2016) to (2.1). It is worth noting that the bounds for the rapidly rotating limit in RBC apply to arbitrary Pr, making the results relevant for geophysical flows. However, for geophysical applications, in addition to rapid rotation, IHC in spherical geometry is of importance. No rigorous study on the turbulent state of such a system is known, and any change in the bounds with a variation in the geometry is an intriguing avenue for future research.

For any result obtained with a bounding method, an important question is on the sharpness of the bounds. High-resolution numerical simulations can provide insight into the sharpness of the bounds in (1). A numerical study of the parameter space would provide valuable insight into the nature of heat transport in uniform rotating IHC, as no such data, numerical and experimental, exists to the best of the author's knowledge on IHC. Then, proof of better bounds, by moving away from quadratic auxiliary functionals, and hence the background field method, can also answer the question of sharpness. In general, mathematical improvements are obtained in one of two ways: either by changes to the variational problem, such that the expressions for the bounds and the spectral constraint change, or by novel estimates of the flow quantities. The latter method is more mathematically challenging, while the prior can be achieved with new physical insights. For example, given that additional constraints, such as minimum and maximum principles, improve bounds for convection (Otto & Seis 2011; Arslan *et al.* 2021*b*), it would be interesting to see if information about rotation can be exploited to construct a variational problem from (2.1), that yields better bounds. Beyond the relation between the R_L and E, a trait of rotating flows is the Taylor–Proudman theorem, which could form the basis of an additional constraint which improves the bounds. In addition, alternative auxiliary functionals might bear fruit in studying bounds on rotating convection. More concretely, the linear stability analysis reveals the importance of the vertical vorticity, and functionals that incorporate vorticity may provide insight into improved bounds, especially given the conjecture in Chernyshenko (2023) for the use of helicity in the auxiliary functional. Similar functionals appear in studies on nonlinear stability of rotating RBC (Galdi & Straughan 1985; Giacobbe & Mulone 2014).

As a final remark, recent work has highlighted novel results when the internal heating is non-uniform (Lepot, Aumaître & Gallet 2018; Bouillaut *et al.* 2022; Song, Fantuzzi & Tobasco 2022; Arslan *et al.* 2024). The change in the physics or bounds due to distributed heating or cooling would be an interesting future line of research. From the perspective of

Bound	Equation	Constant	Value
$\mathcal{F}_B$	(4.47)	d_1	$\frac{18-7\sqrt{3}}{36}(\frac{7\sqrt{6}}{16c_2})^{2/3}$
	(4.47)	d_2	$\frac{1}{12}(\frac{1}{6})^{1/12}\sqrt{\frac{21}{c_2}}$
	(4.47)	d_3	$(\frac{7\sqrt{6}}{12c_2})^{1/3}$
	(4.47)	d_4	$\frac{18-7\sqrt{3}}{36}(\frac{49\sqrt{2}}{2c_2^2})^{1/3}$
	(4.47)	d_5	$\frac{\sqrt{7}}{3}(\frac{9}{32\sqrt{2}c_2^5})^{1/12}$
	(4.47)	d_6	$(\frac{392\sqrt{2}}{9c_2^2})^{1/6}$
	(4.67)	d_7	$\frac{\sqrt{3}\pi(18-7\sqrt{3})}{96}$
	(4.67)	d_8	$\frac{(\sqrt{3}\pi)^{4/5}}{2^{14/5}}$
	(4.67)	d_9	$(\frac{\sqrt{3}\pi}{2})^{2/5}$
$\overline{\langle T\rangle}$	(5.23)	d_{10}	$\frac{2}{9}(\frac{7\sqrt{2}}{8c_2})^{2/7}$
	(5.23)	d_{11}	$\frac{2}{9}(\frac{196}{c_2^2})^{1/7}$
	(5.34)	d_{12}	$\frac{2}{9}(\frac{9\pi}{8})^{1/3}$
	(5.34)	d_{13}	$\frac{1}{6}$

the PDE, extending the set-up in (2.1*c*) to arbitrary heating profiles would be the natural next step when studying bounds on the long-time behaviour of turbulence.

Acknowledgements. The author thanks Andrew Jackson for valuable discussions, insights and for commenting on the manuscript and Fabian Burnman for reading and commenting on the manuscript.

Funding. The author acknowledges funding from the European Research Council (agreement no. 833848-UEMHP) under the Horizon 2020 program and the Swiss National Science Foundation (grant number 219247) under the MINT 2023 call.

Declaration of interests. The author reports no conflict of interest.

Author ORCID.
Ali Arslan https://orcid.org/0000-0002-5824-5604.

Appendix A. Table of constants

For clarity in the proofs of the lower bounds on $\mathcal{F}_B$ and $\overline{\langle T\rangle}$ ((4.47), (4.67), (5.23) and (5.34)), collated here are the constants that appear in the bounds. References to the precise equations where they appear are included.

Appendix B. Heuristics scaling arguments

Owing to the lack of data on uniform IHC subject to rotation, we cannot comment on the sharpness of the bounds proven. Instead, we can use standard physical arguments to determine possible scaling laws for $\overline{\langle T\rangle}$ and $\mathcal{F}_B$. In previous studies, the theory of Grossman & Lohse (see Grossmann & Lohse 2000; Ahlers, Grossmann & Lohse 2009) has been adapted to uniform and exponentially varying IHC to determine scaling laws

in the non-rotating case (Creyssels 2020, 2021; Wang, Lohse & Shishkina 2020). Here, we follow the heuristic arguments presented in Arslan *et al.* (2021*b*) that adapt the ideas of marginal stability and diffusivity-free scaling of Malkus (1954) and Spiegel (1963). Heuristic arguments can be adapted to the rotating case to propose possible scaling laws for rotation-dominated convection (King *et al.* 2009; Aurnou *et al.* 2020; Ecke & Shishkina 2023).

The starting point is to suppose that the heat fluxes out of the domain, defined in (1.1), can be written as $\mathcal{F}_B \sim \overline{\langle T \rangle}/\delta$ and $\mathcal{F}_T \sim \overline{\langle T \rangle}/\varepsilon$. Once again, δ and ε are the thermal boundary layer thicknesses at the bottom and top and are different sizes. In this section, $\sim$ means approximately equal to up to constants. Then, in the buoyancy and rotation-dominated regimes, we assume that to the highest order, the mean temperature is a function of the Rayleigh and Ekman numbers, more precisely

$$\overline{\langle T \rangle} \sim R^{-\alpha} \quad \text{and} \quad \overline{\langle T \rangle} \sim (R/R_L)^{-\gamma} = R^{-\gamma} E^{-4\gamma/3}, \tag{B1a,b}$$

where $\alpha \in \mathbb{R}_+$ and $\gamma \in \mathbb{R}_+$ are exponents to be determined and we have substituted for R_L with (3.15). The assumption (B1) is justified in the non-rotating case by numerical studies of $\overline{\langle T \rangle}$ (Goluskin 2015, table 3.2 and references therein).

The two main regimes of buoyancy and rotation-dominated turbulent convection can be interpolated by varying the Rayleigh and Ekman numbers. However, in going from buoyancy to rotation-dominated heat transport, the thermal boundary layer will become larger than the Ekman boundary layer. However, first, we need to determine the behaviour of the thermal boundary layers. One possible argument, but by no means the only one, is the following. In the bottom boundary, heating balances diffusion, given that the flow is stably stratified. Then, heating over δ is proportional to δ while diffusion scales as $\overline{\langle T \rangle}/\delta$, implying that $\delta^2 \sim \overline{\langle T \rangle}$ and by the energy balance of $\mathcal{F}_T + \mathcal{F}_B = 1$ that $\delta^2 \sim \varepsilon$. Stated in words, the upper thermal boundary layer scales as the mean temperature and is the square of the lower thermal boundary layer. The implication is that $\mathcal{F}_B \sim \overline{\langle T \rangle}^{1/2}$. Turning to the Ekman boundary layers, by standard arguments $\delta_E \sim E^{1/2}$ (Stevenson 1979). Therefore, using (B1) and supposing $\delta \sim \delta_E$, the resulting algebraic equation gives

$$\gamma = \frac{3\alpha}{3 - 4\alpha}. \tag{B2}$$

The relationship in (B2) gives a range of possible scaling behaviours for the IHC as the flow transitions from buoyancy to rotation-dominated, and it then remains to determine α. If we first rearrange (B2) in terms of α, we find that $\alpha = 3\gamma/(3 + 4\gamma)$. For $\gamma \to \infty$, then $\alpha \to \frac{3}{4}$, and the maximal exponent of α is $\frac{3}{4}$, but this does not correspond to any physical arguments and is ruled out by rigorous bounds (Lu *et al.* 2004; Whitehead & Doering 2011*a*).

It remains to determine α to obtain the desired heuristic scaling laws. If we use the argument of marginal stability (Malkus 1954; Howard 1963) to the unstably stratified upper thermal boundary layer, ε, we find that $\alpha = \frac{1}{4}$ and call this the classical exponent. If, instead, turbulent heat transport is independent of the fluid diffusivities and is given by a characteristic free-fall velocity (Spiegel 1963), we find $\alpha = \frac{1}{3}$ and refer to this as the ultimate exponent. See Arslan *et al.* (2021*b*) for a detailed explanation of the exponents for IHC in the non-rotating case. Then, for $\alpha = \frac{1}{4}$ or $\frac{1}{3}$, using (B2) gives the following predictions in the buoyancy and rotation-dominated regimes,

$$\text{non-rotating}: \quad \overline{\langle T \rangle} \sim \begin{cases} R^{-1/4}, & \text{classical}, \\ R^{-1/3}, & \text{ultimate}, \end{cases} \tag{B3a}$$

$$\text{rotating}: \quad \overline{\langle T \rangle} \sim \begin{cases} R^{-3/8}E^{-1/2}, & \text{classical}, \\ R^{-3/5}E^{-4/5}, & \text{ultimate}, \end{cases} \tag{B3b}$$

and

$$\text{non-rotating}: \quad \mathcal{F}_B \sim \begin{cases} R^{-1/8}, & \text{classical}, \\ R^{-1/6}, & \text{ultimate}, \end{cases} \tag{B4a}$$

$$\text{rotating}: \quad \mathcal{F}_B \sim \begin{cases} R^{-3/16}E^{-1/4}, & \text{classical}, \\ R^{-3/10}E^{-2/5}, & \text{ultimate}. \end{cases} \tag{B4b}$$

While the classical regime for a rotating flow is not physically relevant (Ecke & Shishkina 2023), it appears in (B3*b*) and (B4*b*) for completeness.

As mentioned in the introduction, one can define a proxy Nusselt number as $Nu_p = 1/\overline{\langle T \rangle}$. Furthermore, the temperature-difference-based Rayleigh number, Ra, appearing in studies of boundary-driven thermal convection, is related to the flux-based Rayleigh number, R, through the relation that $Nu_p = R/Ra$. Therefore, substituting for R in the scaling laws (B3*a*) and (B3*b*) returns the known scaling laws for the Nusselt number in RBC of $Nu \sim Ra^{1/2}$ and $Nu \sim Ra^{3/2}E^2$ for the ultimate scaling. We comment on the heuristic scaling laws in § 6 and compare them with the bounds we prove in the subsequent sections.

References

Ahlers, G., Grossmann, S. & Lohse, D. 2009 Heat transfer and large scale dynamics in turbulent Rayleigh–Bénard convection. *Rev. Mod. Phys.* **81** (2), 503–537.

Arslan, A., Fantuzzi, G., Craske, J. & Wynn, A. 2021*a* Bounds for internally heated convection with fixed boundary heat flux. *J. Fluid Mech.* **992**, R1.

Arslan, A., Fantuzzi, G., Craske, J. & Wynn, A. 2021*b* Bounds on heat transport for convection driven by internal heating. *J. Fluid Mech.* **919**, A15.

Arslan, A., Fantuzzi, G., Craske, J. & Wynn, A. 2023 Rigorous scaling laws for internally heated convection at infinite Prandtl number. *J. Math. Phys.* **64** (2), 023101.

Arslan, A., Fantuzzi, G., Craske, J. & Wynn, A. 2024 Internal heating profiles for which downward conduction is impossible. *J. Fluid Mech.* **993**, A5.

Arslan, A. & Rojas, R.E. 2024 New bounds for heat transport in internally heated convection at infinite Prandtl number. arXiv:2403.14407.

Aurnou, J.M., Horn, S. & Julien, K. 2020 Connections between nonrotating, slowly rotating, and rapidly rotating turbulent convection transport scalings. *Phys. Rev. Res.* **2** (4), 043115.

Barker, A.J., Dempsey, A.M. & Lithwick, Y. 2014 Theory and simulations of rotating convection. *Astrophys. J.* **791** (1), 13.

Boubnov, B.M. & Golitsyn, G.S. 2012 *Convection in Rotating Fluids*. Springer Science & Business Media.

Bouillaut, V., Flesselles, B., Miquel, B., Aumaître, S. & Gallet, B. 2022 Velocity-informed upper bounds on the convective heat transport induced by internal heat sources and sinks. *Phil. Trans. R. Soc.* A **380** (2225), 20210034.

Busse, F.H. 1970 Bounds for turbulent shear flow. *J. Fluid Mech.* **41** (1), 219–240.

Chandrasekhar, S. 1961 *Hydrodynamic and Hydromagnetic Stability*. Oxford University Press.

Chernyshenko, S. 2022 Relationship between the methods of bounding time averages. *Phil. Trans. R. Soc.* A **380** (1), 20210044.

Chernyshenko, S. 2023 Background flow hidden in a bound for Nusselt number. *Physica* D*: Nonlinear Phenom.* **445**, 133641.

Chernyshenko, S., Goulart, P.J., Huang, D. & Papachristodoulou, A. 2014 Polynomial sum of squares in fluid dynamics: a review with a look ahead. *Phil. Trans. R. Soc.* A **372** (2020), 20130350.

Constantin, P. 1994 Geometric statistics in turbulence. *SIAM Rev.* **36** (1), 73–98.

CONSTANTIN, P. & DOERING, C.R. 1995 Variational bounds on energy dissipation in incompressible flows. II. Channel flow. *Phys. Rev.* E **51** (4), 3192–3198.

CONSTANTIN, P., HALLSTROM, C. & POUTKARADZE, V. 2001 Logarithmic bounds for infinite Prandtl number rotating convection. *J. Math. Phys.* **42** (2), 773–783.

CONSTANTIN, P., HALLSTROM, C. & PUTKARADZE, V. 1999 Heat transport in rotating convection. *Physica* D*: Nonlinear Phenom.* **125** (3-4), 275–284.

CREYSSELS, M. 2020 Model for classical and ultimate regimes of radiatively driven turbulent convection. *J. Fluid Mech.* **900**, A39.

CREYSSELS, M. 2021 Model for thermal convection with uniform volumetric energy sources. *J. Fluid Mech.* **919**, A13.

CURRIE, L.K., BARKER, A.J., LITHWICK, Y. & BROWNING, M.K. 2020 Convection with misaligned gravity and rotation: simulations and rotating mixing length theory. *Mon. Not. R. Astron. Soc.* **493** (4), 5233–5256.

DAVIS, S.H. 1969 On the principle of exchange of stabilities. *Proc. R. Soc. Lond.* A *Math. Phys. Sci.* **310** (1502), 341–358.

DING, Z. & MARENSI, E. 2019 Upper bound on angular momentum transport in Taylor–Couette flow. *Phys. Rev.* E **100** (6), 063109.

DOERING, C.R. 2020 Turning up the heat in turbulent thermal convection. *Proc. Natl Acad. Sci.* **117** (18), 9671–9673.

DOERING, C.R. & CONSTANTIN, P. 1992 Energy dissipation in shear driven turbulence. *Phys. Rev. Lett.* **69** (11), 1648.

DOERING, C.R. & CONSTANTIN, P. 1994 Variational bounds on energy dissipation in incompressible flows: shear flow. *Phys. Rev.* E **49** (5), 4087–4099.

DOERING, C.R. & CONSTANTIN, P. 1996 Variational bounds on energy dissipation in incompressible flows. III. Convection. *Phys. Rev.* E **53** (6), 5957–5981.

DOERING, C.R. & CONSTANTIN, P. 2001 On upper bounds for infinite Prandtl number convection with or without rotation. *J. Math. Phys.* **42** (2), 784–795.

DOERING, C.R., OTTO, F. & REZNIKOFF, M.G. 2006 Bounds on vertical heat transport for infinite Prandtl number Rayleigh–Bénard convection. *J. Fluid Mech.* **560**, 229–241.

ECKE, R.E. & SHISHKINA, O. 2023 Turbulent rotating Rayleigh–Bénard convection. *Annu. Rev. Fluid Mech.* **55**, 603–638.

FANTUZZI, G. 2018 Bounds for Rayleigh–Bénard convection between free-slip boundaries with an imposed heat flux. *J. Fluid Mech.* **837**, R5.

FANTUZZI, G., ARSLAN, A. & WYNN, A. 2022 The background method: theory and computations. *Phil. Trans. R. Soc.* A **380** (1), 20210038.

FANTUZZI, G. & WYNN, A. 2016 Optimal bounds with semidefinite programming: an application to stress-driven shear flows. *Phys. Rev.* E **93** (4), 043308.

GALDI, G.P. & STRAUGHAN, B. 1985 A nonlinear analysis of the stabilizing effect of rotation in the Bénard problem. *Proc. R. Soc. Lond.* A *Math. Phys. Sci.* **402** (1823), 257–283.

GIACOBBE, A. & MULONE, G. 2014 Stability in the rotating Benard problem and its optimal Lyapunov functions. *Acta Appl. Math.* **132**, 307–320.

GLATZMAIER, G. 2013 *Introduction to Modeling Convection in Planets and Stars: Magnetic Field, Density Stratification, Rotation*. Princeton University Press.

GOLUSKIN, D. 2015 *Internally Heated Convection and Rayleigh–Bénard Convection*. Springer.

GOLUSKIN, D. & VAN DER POEL, E.P. 2016 Penetrative internally heated convection in two and three dimensions. *J. Fluid Mech.* **791**, R6.

GOLUSKIN, D. & SPIEGEL, E.A. 2012 Convection driven by internal heating. *Phys. Lett.* A **377** (1-2), 83–92.

GREENSPAN, H.P. 1968 *The Theory of Rotating Fluids*. Cambridge University Press.

GROOMS, I., JULIEN, K., WEISS, J.B. & KNOBLOCH, E. 2010 Model of convective Taylor columns in rotating Rayleigh–Bénard convection. *Phys. Rev. Lett.* **104** (22), 224501.

GROOMS, I. & WHITEHEAD, J.P. 2014 Bounds on heat transport in rapidly rotating Rayleigh–Bénard convection. *Nonlinearity* **28** (1), 29.

GROSSMANN, S. & LOHSE, D. 2000 Scaling in thermal convection: a unifying theory. *J. Fluid Mech.* **407**, 27–56.

GUERVILLY, C. & CARDIN, P. 2016 Subcritical convection of liquid metals in a rotating sphere using a quasi-geostrophic model. *J. Fluid Mech.* **808**, 61–89.

GUZMÁN, A.J.A., MADONIA, M., CHENG, J.S., OSTILLA-MÓNICO, R., CLERCX, H.J.H. & KUNNEN, R.P.J. 2020 Competition between Ekman plumes and vortex condensates in rapidly rotating thermal convection. *Phys. Rev. Lett.* **125** (21), 214501.

HADJERCI, G., BOUILLAUT, V., MIQUEL, B. & GALLET, B. 2024 Rapidly rotating radiatively driven convection: experimental and numerical validation of the 'geostrophuc turbulence' scaling predictions. arXiv:2401.16200.

HERANT, M., BENZ, W., HIX, W.R., FRYER, C.L. & COLGATE, S.A. 1994 Inside the supernova: a powerful convective engine. *Astrophys. J.* **435**(1), 339–361.

HERRON, I.H. 2003 On the principle of exchange of stabilities in Rayleigh–Bénard convection, II-no-slip boundary conditions. *Ann. Univ. Ferrara* **49**, 169–182.

HOWARD, L.N. 1963 Heat transport by turbulent convection. *J. Fluid Mech.* **17** (3), 405–432.

JONES, C.A. & SCHUBERT, G. 2015 Thermal and compositional convection in the outer core. *Treat. Geophys. Core Dyn.* **8**, 131–185.

JONES, C.A., SOWARD, A.M. & MUSSA, A.I. 2000 The onset of thermal convection in a rapidly rotating sphere. *J. Fluid Mech.* **405**, 157–179.

JULIEN, K., AURNOU, J.M., CALKINS, M.A., KNOBLOCH, E., MARTI, P., STELLMACH, S. & VASIL, G.M. 2016 A nonlinear model for rotationally constrained convection with Ekman pumping. *J. Fluid Mech.* **798**, 50–87.

JULIEN, K., LEGG, S., MCWILLIAMS, J. & WERNE, J. 1996 Rapidly rotating turbulent Rayleigh–Bénard convection. *J. Fluid Mech.* **322**, 243–273.

JULIEN, K., RUBIO, A.M., GROOMS, I. & KNOBLOCH, E. 2012 Statistical and physical balances in low Rossby number Rayleigh–Bénard convection. *Geophys. Astrophys. Fluid Dyn.* **106** (4–5), 392–428.

KAPLAN, E.J., SCHAEFFER, N., VIDAL, J. & CARDIN, P. 2017 Subcritical thermal convection of liquid metals in a rapidly rotating sphere. *Phys. Rev. Lett.* **119** (9), 094501.

KING, E.M., STELLMACH, S. & BUFFETT, B. 2013 Scaling behaviour in Rayleigh–Bénard convection with and without rotation. *J. Fluid Mech.* **717**, 449–471.

KING, E.M., STELLMACH, S., NOIR, J., HANSEN, U. & AURNOU, J.M. 2009 Boundary layer control of rotating convection systems. *Nature* **457** (7227), 301–304.

KNOBLOCH, E. 1998 Rotating convection: recent developments. *Intl J. Engng Sci.* **36** (12–14), 1421–1450.

KUMAR, A. 2022 Geometrical dependence of optimal bounds in Taylor–Couette flow. *J. Fluid Mech.* **948**, A11.

KUMAR, A., ARSLAN, A., FANTUZZI, G., CRASKE, J. & WYNN, A. 2022 Analytical bounds on the heat transport in internally heated convection. *J. Fluid Mech.* **938**, A26.

KUNNEN, R.P.J. 2021 The geostrophic regime of rapidly rotating turbulent convection. *J. Turbul.* **22** (4–5), 267–296.

LEPOT, S., AUMAÎTRE, S. & GALLET, B. 2018 Radiative heating achieves the ultimate regime of thermal convection. *Proc. Natl Acad. Sci. USA* **115** (36), 8937–8941.

LU, L., DOERING, C.R. & BUSSE, F.H. 2004 Bounds on convection driven by internal heating. *J. Math. Phys.* **45** (7), 2967–2986.

MALKUS, W.V.R. 1954 The heat transport and spectrum of thermal turbulence. *Proc. R. Soc.* A **225** (1161), 196–212.

MULYUKOVA, E. & BERCOVICI, D. 2020 Mantle convection in terrestrial planets. Oxford Research Encyclopedia of Planetery Sciences.

NOBILI, C. 2023 The role of boundary conditions in scaling laws for turbulent heat transport. *Math. Engng* **5** (1), 1–41.

OTTO, F. & SEIS, C. 2011 Rayleigh–Bénard convection: improved bounds on the nusselt number. *J. Math. Phys.* **52** (8), 083702.

PACHEV, B., WHITEHEAD, J.P., FANTUZZI, G. & GROOMS, I. 2020 Rigorous bounds on the heat transport of rotating convection with Ekman pumping. *J. Math. Phys.* **61** (2), 023101.

PLUMLEY, M. & JULIEN, K. 2019 Scaling laws in Rayleigh–Bénard convection. *Earth Space Sci.* **6** (9), 1580–1592.

RADICE, D., OTT, C.D., ABDIKAMALOV, E., COUCH, S.M., HAAS, R. & SCHNETTER, E. 2016 Neutrino-driven convection in core-collapse supernovae: high-resolution simulations. *Astrophys. J.* **820** (1), 76.

ROBERTS, P.H. 1967 Convection in horizontal layers with internal heat generation. Theory. *J. Fluid Mech.* **30** (1), 33–49.

ROBERTS, P.H. 1968 On the thermal instability of a rotating-fluid sphere containing heat sources. *Phil. Trans. R. Soc. Lond.* A **263** (1136), 93–117.

ROSA, R.M.S. & TEMAM, R.M. 2022 Optimal minimax bounds for time and ensemble averages of dissipative infinite-dimensional systems with applications to the incompressible Navier–Stokes equations. *Pure Appl. Funct. Anal.* **7** (1), 327–355.

ROSSBY, H.T. 1969 A study of Bénard convection with and without rotation. *J. Fluid Mech.* **36** (2), 309–335.

SCHUBERT, G. 2015 *Treatise on Geophysics*. Elsevier.
SCHUBERT, G., TURCOTTE, D.L. & OLSON, P. 2001 *Mantle Convection in the Earth and Planets*. Cambridge University Press.
SCHUMACHER, J. & SREENIVASAN, K.R. 2020 Colloquium: unusual dynamics of convection in the Sun. *Rev. Mod. Phys.* **92**, 041001.
SONG, B., FANTUZZI, G. & TOBASCO, I. 2022 Bounds on heat transfer by incompressible flows between balanced sources and sinks. *Physica* D*: Nonlinear Phenom.* **444**, 133591.
SONG, J., SHISHKINA, O. & ZHU, X. 2024 Scaling regimes in rapidly rotating thermal convection at extreme Rayleigh numbers. *J. Fluid Mech.* **984**, A45.
SPIEGEL, E.A. 1963 A generalization of the mixing-length theory of turbulent convection. *Astrophys. J.* **138**, 216.
SPRAGUE, M., JULIEN, K., KNOBLOCH, E. & WERNE, J. 2006 Numerical simulation of an asymptotically reduced system for rotationally constrained convection. *J. Fluid Mech.* **551**, 141–174.
STELLMACH, S., LISCHPER, M., JULIEN, K., VASIL, G., CHENG, J.S., RIBEIRO, A., KING, E.M. & AURNOU, J.M. 2014 Approaching the asymptotic regime of rapidly rotating convection: boundary layers versus interior dynamics. *Phys. Rev. Lett.* **113** (25), 254501.
STEVENS, R.J.A.M., VAN DER POEL, E.P., GROSSMANN, S. & LOHSE, D. 2013 The unifying theory of scaling in thermal convection: the updated prefactors. *J. Fluid Mech.* **730**, 295–308.
STEVENSON, D.J. 1979 Turbulent thermal convection in the presence of rotation and a magnetic field: a heuristic theory. *Geophys. Astrophys. Fluid Dyn.* **12** (1), 139–169.
STRAUGHAN, B. 2013 *The Energy Method, Stability, and Nonlinear Convection*, vol. 91. Springer Science & Business Media.
TILGNER, A. 2022 Bounds for rotating Rayleigh–Bénard convection at large Prandtl number. *J. Fluid Mech.* **930**, A33.
TOBASCO, I., GOLUSKIN, D. & DOERING, C.R. 2018 Optimal bounds and extremal trajectories for time averages in nonlinear dynamical systems. *Phys. Lett.s* A **382** (6), 382–386.
VERONIS, G. 1959 Cellular convection with finite amplitude in a rotating fluid. *J. Fluid Mech.* **5** (3), 401–435.
VOROBIEFF, P. & ECKE, R.E. 2002 Turbulent rotating convection: an experimental study. *J. Fluid Mech.* **458**, 191–218.
WANG, Q., LOHSE, D. & SHISHKINA, O. 2020 Scaling in internally heated convection: a unifying theory. *Geophys. Res. Lett.* **47**, e2020GL091198.
WANG, X. 2007 Asymptotic behavior of the global attractors to the Boussinesq system for Rayleigh–Bénard convection at large Prandtl number. *Commun. Pure. Appl. Math.* **60** (9), 1293–1318.
WANG, X. & WHITEHEAD, J.P. 2013 A bound on the vertical transport of heat in the 'ultimate' state of slippery convection at large Prandtl numbers. *J. Fluid Mech.* **729**, 103–122.
WHITEHEAD, J.P. & DOERING, C.R. 2011*a* Internal heating driven convection at infinite Prandtl number. *J. Math. Phys.* **52** (9), 093101.
WHITEHEAD, J.P. & DOERING, C.R. 2011*b* Ultimate state of two-dimensional Rayleigh–Bénard convection between free-slip fixed-temperature boundaries. *Phys. Rev. Lett.* **106** (24), 244501.
WHITEHEAD, J.P. & DOERING, C.R. 2012 Rigid bounds on heat transport by a fluid between slippery boundaries. *J. Fluid Mech.* **707**, 241–259.
YAN, X. 2004 On limits to convective heat transport at infinite Prandtl number with or without rotation. *J. Math. Phys.* **45** (7), 2718–2743.